Article

Developmental Cell

CEH-60/PBX and UNC-62/MEIS Coordinate a Metabolic Switch that Supports Reproduction in *C. elegans*

Graphical Abstract

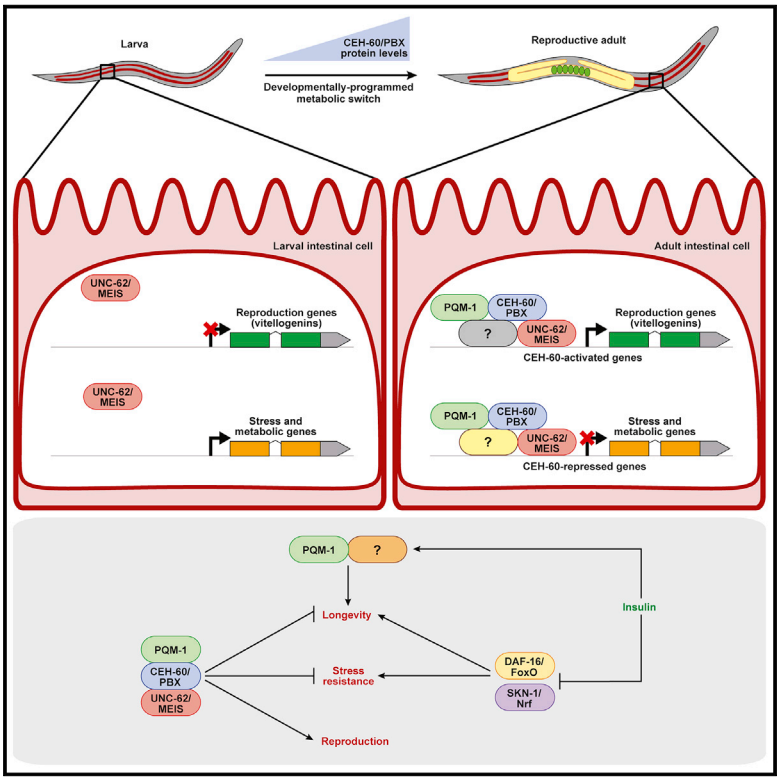

Highlights

- CEH-60/PBX associates with UNC-62/MEIS to control gene expression in *C. elegans*
- The CEH-60:UNC-62 dimer activates and represses transcription in intestinal nuclei
- CEH-60 represses longevity and stress genes while activating reproduction genes
- CEH-60 interacts with PQM-1 at GATA sequences to repress gene expression

Authors

Robert H. Dowen

Correspondence

dowen@email.unc.edu

In Brief

Reproductive success often occurs at the expense of longevity and stress resistance. Dowen identifies two key molecular regulators of this trade-off, CEH-60/PBX and UNC-62/MEIS, in *C. elegans*. These transcription factors function together to balance the allocation of lipid resources between somatic and germline functions to ensure organismal energy homeostasis.

Dowen, 2019, Developmental Cell *49*, 235–250
April 22, 2019
https://doi.org/10.1016/j.devcel.2019.03.002

CellPress

Developmental Cell
Article

CEH-60/PBX and UNC-62/MEIS Coordinate a Metabolic Switch that Supports Reproduction in *C. elegans*

Robert H. Dowen[1,2,*]
[1]Integrative Program for Biological and Genome Sciences, The University of North Carolina at Chapel Hill, Chapel Hill, NC 27599, USA
[2]Lead Contact
*Correspondence: dowen@email.unc.edu
https://doi.org/10.1016/j.devcel.2019.03.002

SUMMARY

The molecular basis of how animals integrate metabolic, developmental, and environmental information before committing resources to reproduction is an unresolved issue in developmental biology. In *C. elegans*, adult animals reallocate fat stores from intestinal cells to the germline via low-density lipoprotein (LDL)-like particles to promote embryogenesis. Here, I demonstrate that two conserved homeodomain transcription factors, CEH-60/PBX and UNC-62/MEIS, coordinate a transcriptional network that supports reproduction while suppressing longevity and stress-response pathways. The CEH-60:UNC-62 heterodimer serves an unanticipated dual function in intestinal nuclei by directly activating the expression of lipoprotein genes while directly repressing stress-responsive genes. Consequently, *ceh-60* mutants display fat storage defects, a dramatic lifespan extension, and hyper-activation of innate immunity genes. Finally, CEH-60 associates with PQM-1 at the DAF-16-associated element within the promoters of stress-responsive genes to control gene expression. Thus, CEH-60 governs an elaborate transcriptional network that balances stress responses and longevity against reproduction during developmental transitions.

INTRODUCTION

Animals must effectively manage energy reserves to ensure viability and optimize reproduction in the face of environmental challenges. Balancing vital resources between somatic and germline functions is integral to the survival of a species. As a general feature of metazoans, reallocation of energy stores from somatic tissues to the germline ensures reproductive robustness. In *Caenorhabditis elegans*, the transition from developing larva to reproductive adult is marked by a dramatic redistribution of intestinal lipids to the germline. The developmental switch that underlies this metabolic trade-off supports fecundity while restricting somatic longevity (O'Rourke et al., 2009; Arantes-Oliveira et al., 2002); however, the regulatory mechanisms that coordinate resource allocation remain poorly understood.

Proper allocation of energy reserves between somatic and germline tissues is thought to modulate, at least in part, a trade-off between longevity and reproductive fitness, a model that is described by the "disposable soma" theory of aging (Kirkwood and Holliday, 1979; Kirkwood, 1977). During reproduction, highly abundant vitellogenin lipoproteins package intestinal lipids into low-density lipoprotein (LDL) particles that are secreted, captured and endocytosed by the oocyte-specific LDL receptor RME-2, and utilized during embryonic development (Grant and Hirsh, 1999). Remarkably, overexpression of a single vitellogenin is sufficient to deplete intestinal fat stores and reduce the lifespan of long-lived mutants (Seah et al., 2016), demonstrating that lipoprotein abundance is integral to organismal homeostasis and underscoring the need for strict lipoprotein regulatory mechanisms. Indeed, vitellogenin gene expression is highly regulated, coordinated by an array of developmental, nutritional, and metabolic signals (Dowen et al., 2016; Goszczynski et al., 2016; Seah et al., 2016; DePina et al., 2011; Murphy et al., 2003). How developmental and metabolic signals are coordinated to mediate a balance between reproduction and somatic maintenance is a critical problem in organismal biology whose molecular basis is not well understood.

The mechanisms that promote longevity also enhance resistance to a variety of stresses (Zhou et al., 2011). A classic arbitrator of longevity and stress resistance is the insulin/IGF-1-like signaling pathway, mediated by the insulin receptor DAF-2 and its downstream kinases AKT-1/2 and SGK-1, which phosphorylate and repress the two pro-longevity, stress-responsive transcription factors DAF-16/FoxO and SKN-1/Nrf by restricting their localization to the cytoplasm (Baumeister et al., 2006). Reduced insulin signaling stimulates nuclear accumulation of DAF-16 and SKN-1, and consequently, widespread activation of stress-response genes (Tullet et al., 2008; Murphy et al., 2003; Lin et al., 2001). In conjunction with DAF-16, the transcriptional regulator PQM-1 participates in *daf-2*-dependent gene regulation and is required for the enhanced longevity and thermotolerance of *daf-2* mutants (Tepper et al., 2013); however, the target genes that PQM-1 regulates to promote longevity and stress resistance are poorly understood. Although several transcriptional activators of longevity and stress-response pathways have been identified, the repressive transcription factors that oppose these factors are largely unknown.

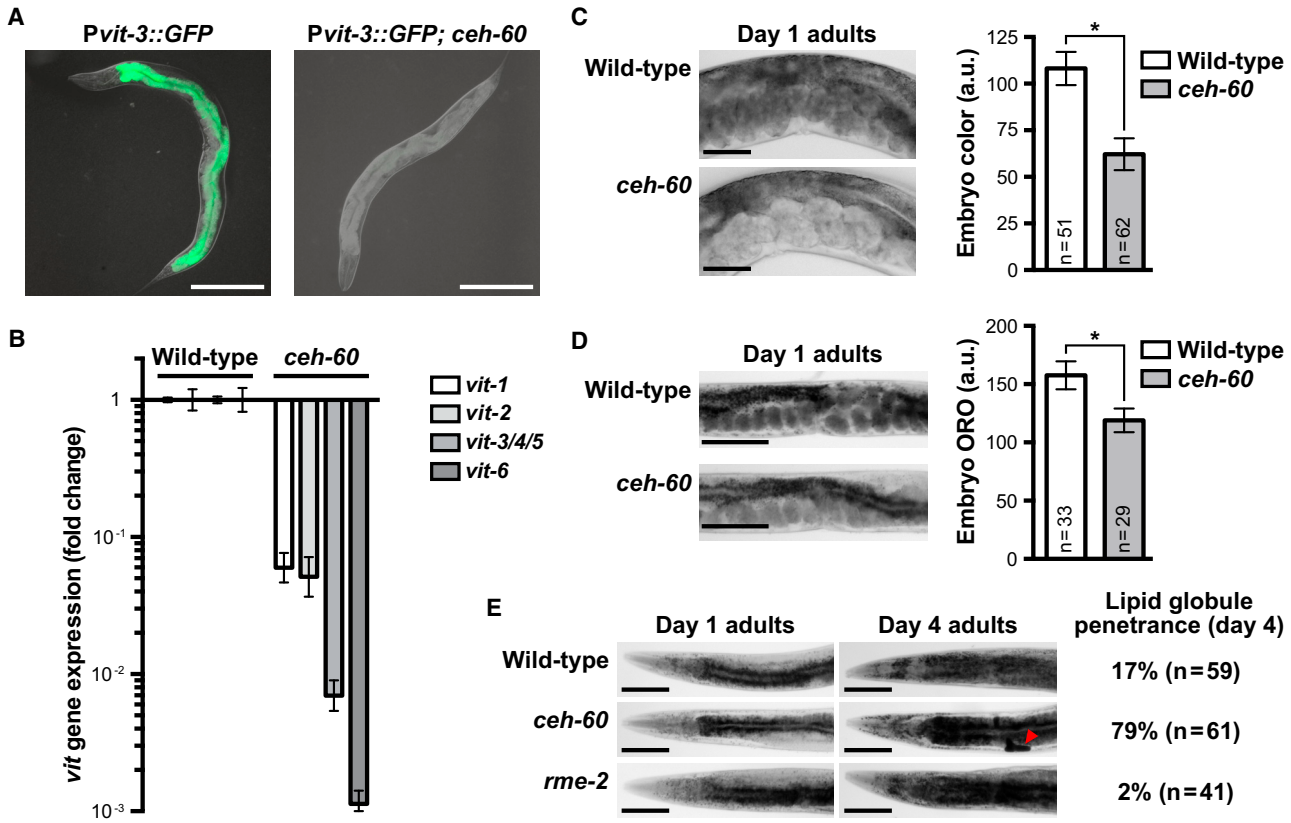

Figure 1. Expression of Intestinal Vitellogenin Requires *ceh-60*

(A) Representative overlaid differential interference contrast (DIC) and GFP fluorescence images of transgenic P*vit-3*::*GFP* or P*vit-3::GFP; ceh-60(ok1485)* day 1 adult animals.

(B) RT-qPCR analysis of endogenous *vit* gene expression in wild-type or *ceh-60(ok1485)* animals. Data are represented relative to wild-type as the mean +/− SEM.

(C) Representative images (left) and quantification (right; mean ± SD; *p < 0.0001, Student's t test) of brightfield micrographs of embryos within the uterus of wild-type or *ceh-60(ok1485)* animals.

(D) Images (left) and quantification (right; mean ± SD; *p < 0.0001, Student's t test) of embryos stained with Oil Red O for the strains in (C).

(E) Micrographs of wild-type, *ceh-60(ok1485)*, and *rme-2(b1008)* animals stained with Oil Red O. The fraction of day 4 adult animals displaying extracellular fat globules is shown for each genotype.

Scale bars: 200 μm in (A) and 100 μm in (C)–(E).

See also Figure S1.

Because of its role in regulating lipoprotein abundance, transcriptional control of vitellogenin expression is likely to be critical for coordinating the trade-off between longevity and reproductive fitness. Here, I identify CEH-60/PBX, a TALE class (Three Amino acid Loop Extension) homeodomain protein within the Pre-B cell leukemia (PBC) transcription factor family, and UNC-62/MEIS, a genetically distinct TALE class homeodomain transcription factor, as key mediators of intestinal resources. As a heterodimeric complex, CEH-60:UNC-62 activates vitellogenin expression while simultaneously repressing the expression of longevity and stress-response genes in the intestine by directly binding to their promoters, indicating that the evolutionarily conserved heterodimer is the elusive transcriptional complex that opposes DAF-16/SKN-1 activity. Moreover, many genes that are directly repressed by CEH-60:UNC-62 are co-regulated by PQM-1, suggesting that the three proteins form a multimeric complex. Thus, CEH-60 is responsible for mediating a developmental transition that devotes resources to reproductive processes while simultaneously dampening longevity and stress-response pathways that are integral to larval development.

RESULTS

CEH-60/PBX Directs Intestinal Fat Transport

Six vitellogenin genes are expressed in the *C. elegans* intestine during the transition from the L4 larval stage into adulthood. Vitellogenin gene expression can be followed using a P*vit-3::GFP* reporter transgene comprised of GFP under control of the *vit-3* promoter (Figure 1A). In an RNAi screen for positive regulators of vitellogenin expression, I previously identified several genes required for activation of the P*vit-3::GFP* reporter (Dowen et al., 2016). One of these genes, *ceh-60*, encodes an evolutionarily conserved homeodomain transcription factor, orthologous to *Drosophila* Extradenticle and mammalian PBX proteins (Figure S1A). To validate this initial observation, I crossed a *ceh-60* loss-of-function mutation into the P*vit-3::GFP* reporter strain,

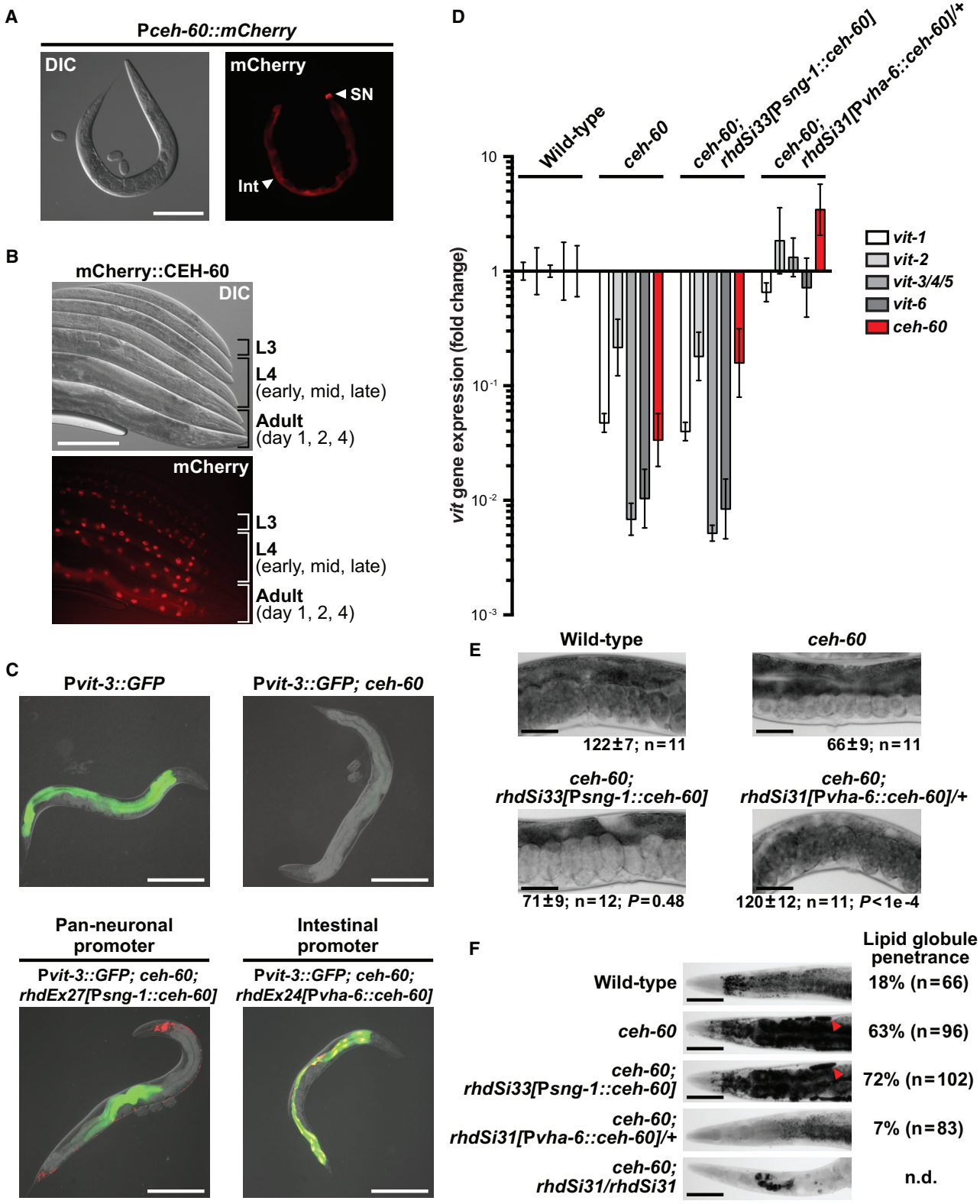

Figure 2. CEH-60 Functions in the Intestine to Regulate Vitellogenesis

(A) Representative DIC and mCherry fluorescence images of a day 1 adult animal carrying an extrachromosomal array expressing P*ceh-60::mCherry* (SN, sensory neurons; Int, intestine).

(legend continued on next page)

which resulted in complete abrogation of intestinal GFP expression at adulthood (Figure 1A). Furthermore, disruption of *ceh-60* resulted in a marked reduction in the expression of the endogenous *vit* genes (10–1,000 fold, Figure 1B). These results highlight a role for CEH-60 in vitellogenesis (Dowen et al., 2016; Van Rompay et al., 2015) and suggest that CEH-60 may function more broadly in energy homeostasis.

Reallocation of intestinal lipids to the germline simultaneously depletes intestinal cells of fat stores while providing the embryo with a key energy source during development. Accordingly, loss of *ceh-60*, which abrogates lipoprotein expression, resulted in mutant embryos that were dramatically lighter in color than wild-type embryos within the hermaphrodite uterus, suggesting that they were largely devoid of lipids (Figure 1C). Consistently, Oil Red O staining of the neutral lipids in the *ceh-60* mutant showed reduced fat levels in embryos, as well as a modest, but reproducible, increase in intestinal fat content as adulthood progressed in a manner similar to the *rme-2* mutant, which lacks the oocyte-specific LDL receptor (Figures 1D, S1B, and S1C). In contrast to the *rme-2* mutants, however, the *ceh-60* animals accumulated extracellular lipid globules by 4 days of adulthood (Figures 1E and S1B). Although the origin of these lipid structures remains unclear, the phenotype is specific to the loss of *ceh-60* and not *rme-2*, suggesting that the globules are not simply a result of vitellogenesis defects.

CEH-60 Functions Cell Autonomously to Regulate Vitellogenesis

Expression of the vitellogenin genes is dynamically controlled by both cell-autonomous and cell-non-autonomous factors (Dowen et al., 2016; Goszczynski et al., 2016; DePina et al., 2011). Previous expression analyses using a transcriptional reporter transgene suggested that *ceh-60* is expressed exclusively in a few sensory neurons in the head (Van Rompay et al., 2015; Reece-Hoyes et al., 2007). However, a *ceh-60* transcriptional reporter constructed with a larger proportion of the putative regulatory sequence revealed that the *ceh-60* promoter is sufficient to drive gene expression in both sensory neurons and the intestine (Figure 2A). Since high-copy overexpression systems can generate expression artifacts, I inserted a 3xHA-mCherry tag into the endogenous *ceh-60* locus using CRISPR/Cas9 to yield an N-terminally tagged fusion protein. Examination of this strain confirmed that *ceh-60* is expressed in the intestine; moreover, it revealed that this expression is temporally restricted, with the mCherry::CEH-60 protein initially accumulating in intestinal nuclei at the L4 larval stage and persisting into adulthood (Figures 2B and S2A).

Intestinal expression of mCherry::CEH-60 at adulthood is consistent with a cell-autonomous role for CEH-60 in lipoprotein regulation. To test this premise, I performed cell-type-specific *ceh-60* rescue experiments. Expression of *ceh-60* in the intestine fully rescued the *ceh-60* mutant defect in P*vit-3::GFP* expression (Figure 2C). To account for potential overexpression artifacts of extrachromosomal arrays, I inserted the rescue constructs as single-copy transgenes into the genome of the *ceh-60* mutant using MosSCI (Frokjaer-Jensen et al., 2008). Expression of the endogenous *vit* genes was severely reduced in the *ceh-60* mutant; however, intestinal rescue of *ceh-60* completely restored *vit* gene expression (Figure 2D). Neuronal overexpression of *ceh-60* using an extrachromosomal array modestly rescued the *ceh-60* mutant defects in P*vit-3::GFP* expression; however, this phenotype was likely an artifact of the array, since a single-copy neuronal rescue transgene failed to restore *vit* gene expression in the *ceh-60* mutant (Figures 2C and 2D). Together, these data demonstrate that intestinal expression of *ceh-60* is sufficient to direct *vit* gene expression. Moreover, knockdown of *ceh-60* exclusively in the intestine, using a tissue-specific RNAi strain (Melo and Ruvkun, 2012), markedly decreased *vit* gene expression (Figure S2B), demonstrating that intestinal expression of *ceh-60* is also necessary for vitellogenin production.

Consistent with these data, intestinal rescue of *ceh-60* restored lipid deposition in the embryo to wild-type levels as well as prevented the accumulation of ectopic extracellular fat globules (Figures 2E, 2F, and S2C). Notably, *ceh-60* mutants that are heterozygous for the intestinal rescue transgene were generally indistinguishable from wild-type animals. In contrast, transgene homozygotes, which presumably express *ceh-60* at higher levels, were small, sterile, and largely devoid of fat (Figure 2F), indicating that *ceh-60* dose may dramatically alter the physiology of the animal, possibly through misregulation of intestinal lipid metabolism genes. Together, these data unambiguously demonstrate an intestinal role for CEH-60 in the regulation of vitellogenesis and lipid homeostasis.

CEH-60 Represses Longevity through a Vitellogenesis-Independent Mechanism

Transcriptional regulators that control vitellogenin expression may function more broadly in organismal development, metabolism, and longevity (Van Nostrand et al., 2013); yet little is known about the mechanisms by which these factors exert their effects. In addition, disruption of vitellogenesis indirectly extends lifespan by activating autophagy and lipolytic pathways (Seah et al., 2016; Murphy et al., 2003). To test the impact of germline

(B) DIC and mCherry fluorescence images showing temporal expression and subcellular localization of an endogenously tagged mCherry::CEH-60 fusion protein in a *glo-4(ok623)* mutant background at the indicated developmental stages.
(C) Overlaid DIC, mCherry, and GFP fluorescence images of wild-type, *ceh-60(ok1485)*, and *ceh-60(ok1485)* transgenic animals carrying tissue-specific rescue constructs as extrachromosomal arrays (mCherry marks the rescued cells). All animals also express P*vit-3::GFP*.
(D) RT-qPCR analysis (mean ± SEM) of *vit* gene expression in wild-type, *ceh-60(ok1485)*, and *ceh-60(ok1485)* rescue strains expressing the constructs in (C) as single-copy integrated transgenes (*rhdSi31*[P*vha-6::ceh-60*]/+ indicates heterozygous for transgene).
(E) Images, quantification (mean ± SD), and statistical analysis (one-way ANOVA relative to *ceh-60*) of brightfield micrographs of embryos in the uterus of day 1 adults for the strains in (D).
(F) Representative images and fat globule penetrance of day 4 adults stained with Oil Red O for those strains in (D). Also shown is an animal homozygous for *rhdSi31* (n.d., not determined).
Scale bars: 200 μm in (A)–(C) and 100 μm in (E) and (F).
See also Figure S2.

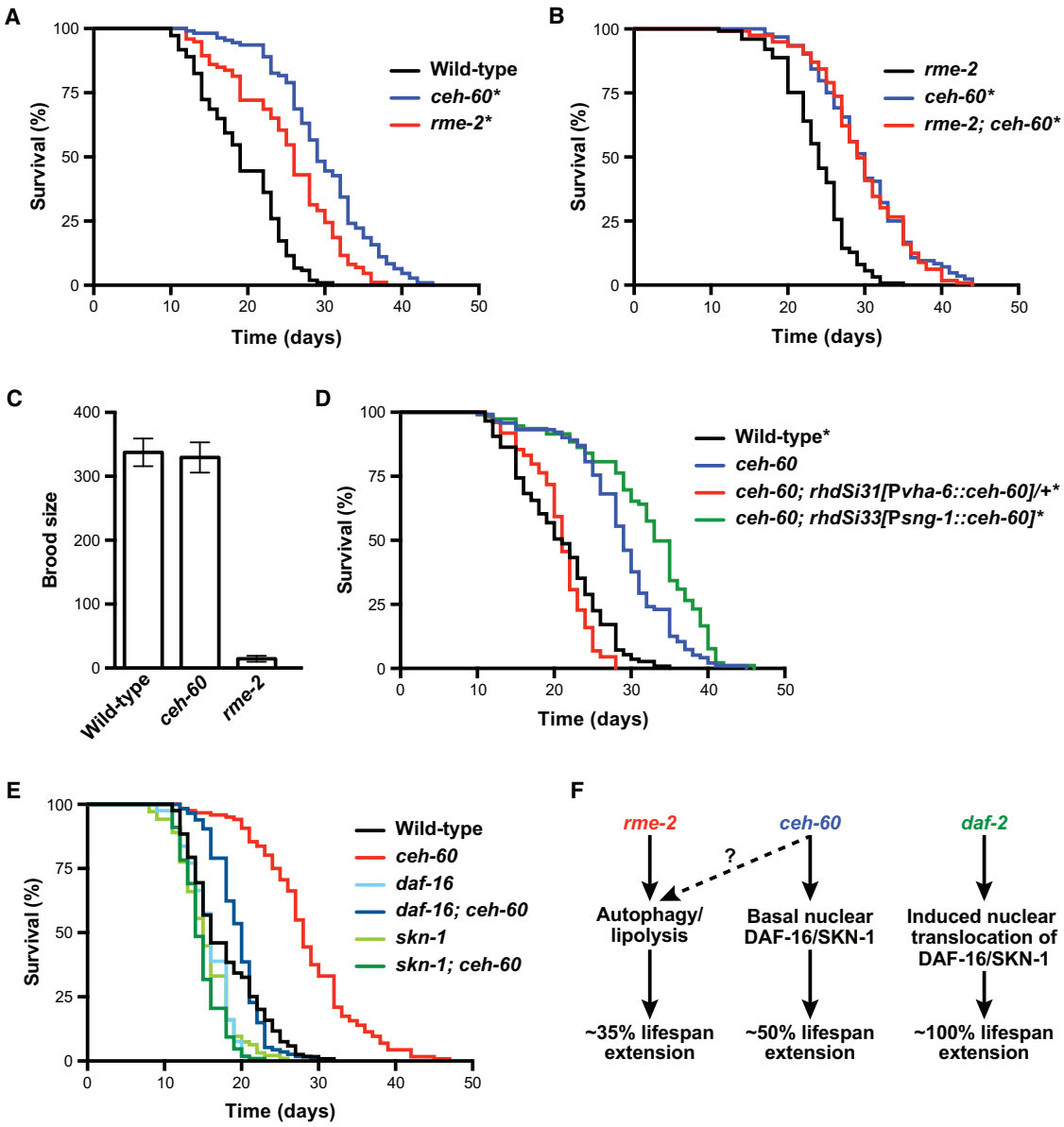

Figure 3. CEH-60 Restricts Lifespan Independently of Vitellogenesis through Canonical Longevity Regulators

(A) Longitudinal lifespan assay showing increased longevity of *rme-2(b1008)* and *ceh-60(ok1485)* mutants relative to wild-type (*p < 0.0001).

(B) Lifespan assay demonstrating *ceh-60(ok1485)* and *rme-2(b1008); ceh-60(ok1485)* double mutants are long-lived relative to *rme-2(b1008)* (*p < 0.0001).

(C) The total number of self-progeny laid (mean +/− SD, 10 individuals per genotype) by those strains in (A).

(D) Longitudinal lifespan of those strains described in Figure 2D (*p < 0.0001, relative to *ceh-60*).

(E) Lifespan assay of wild-type, *ceh-60(ok1485)*, *skn-1(zu135)*, *daf-16(mgDf47)*, *skn-1(zu135); ceh-60(ok1485)*, and *daf-16(mgDf47); ceh-60(ok1485)* animals. All survival curves are significantly different compared with the *ceh-60* curve (p < 0.0001).

(F) A model showing distinct mechanisms of lifespan extension.

See also Figure S3.

vitellogenin deficiency on longevity, I performed longitudinal lifespan assays. Loss of *rme-2*, which encodes the germline LDL receptor that is singularly required for vitellogenin uptake, modestly increased longevity (~35%); however, disruption of *ceh-60* resulted in a more dramatic lifespan extension (~50%, Figure 3A). If the enhanced longevity of the *ceh-60* mutant was simply a product of vitellogenin down-regulation, then loss of *ceh-60* would fail to exacerbate the *rme-2* null mutation; however, *rme-2; ceh-60* double mutants displayed a longer lifespan than the *rme-2* single mutants (p < 0.0001, Figure 3B), indicating that *ceh-60* is epistatic to *rme-2*. This suggests that in wild-type animals, CEH-60 limits lifespan, at least in part, through a vitellogenesis-independent mechanism. Consistent with this model, *ceh-60* mutants produce a wild-type brood size while disruption of *rme-2* severely diminished fertility (Figure 3C). Together, these data clearly demonstrate that loss of *ceh-60* dramatically

enhances longevity without compromising progeny production (see Discussion).

Environmental or genetic factors that influence lifespan can be perceived by and function through various tissues, including sensory neurons and the intestine (Bishop and Guarente, 2007; Libina et al., 2003). Thus, I sought to define the tissue(s) where CEH-60 exerts its longevity effects by determining the lifespan of the *ceh-60* tissue-specific rescue strains. Intestinal, but not neuronal, expression of *ceh-60* was sufficient to fully suppress the enhanced longevity conferred by loss of *ceh-60* (Figure 3D). Consistently, systemic knockdown of *ceh-60* enhanced longevity, which was recapitulated when *ceh-60* was specifically knocked down in the intestine (Figure S3A). Together, these data indicate that intestinal expression of *ceh-60* is both necessary and sufficient to regulate organismal lifespan.

Canonical Regulators of Lifespan Promote Longevity in the Absence of CEH-60

The pro-longevity transcription factors DAF-16/FoxO and SKN-1/Nrf are pivotal regulators of lifespan in response to decreased mTOR (mechanistic target of rapamycin) or insulin-like signaling, both of which function, at least in part, in the intestine to control the expression of longevity and metabolic genes (Robida-Stubbs et al., 2012; Tullet et al., 2008; Libina et al., 2003). To determine whether these canonical transcriptional regulators of longevity pathways are also required for *ceh-60*-dependent lifespan extension, I crossed *skn-1* or *daf-16* null mutations into a *ceh-60* mutant background and performed longitudinal lifespan experiments. Indeed, loss of *daf-16* or *skn-1* partially or completely suppressed the enhanced longevity phenotype of the *ceh-60* mutant, respectively (Figure 3E). In contrast, inactivation of *daf-16* or *skn-1* failed to suppress the vitellogenesis defects or ectopic fat globule accumulation displayed by the *ceh-60* mutant (Figures S3B and S3C), indicating that the lipid and longevity phenotypes are uncoupled in the *ceh-60* mutant. Notably, loss of *ceh-60* failed to enhance the lifespan of the *daf-2(e1370)* mutant (data not shown), suggesting that modifying the activity of CEH-60 may be part of the transcriptional reconfiguration that occurs during reduced insulin conditions.

Reduced insulin signaling in *daf-2* mutants promotes the nuclear accumulation of DAF-16 and SKN-1, promoting widespread up-regulation of longevity and stress-response genes that together dramatically extend lifespan (Tullet et al., 2008; Lin et al., 2001). However, disruption of *ceh-60* failed to promote the accumulation of DAF-16 or SKN-1 protein in the nucleus of intestinal cells at detectable levels (data not shown), suggesting that *ceh-60* mutants employ the basal activities of DAF-16/SKN-1 to extend lifespan during unstressed conditions (Figure 3F).

Dual Functions for CEH-60 in Intestinal Nuclei

To gain mechanistic insight into how CEH-60 simultaneously promotes vitellogenesis and restricts lifespan, I performed whole-transcriptome analysis (mRNA-seq) of wild-type and *ceh-60* mutant animals at days 1 and 4 of adulthood (Figure S4A). Loss of *ceh-60* resulted in mis-expression of 1,927 or 2,112 genes in day 1 or day 4 adults, respectively, with ~70% of those differentially expressed genes being up-regulated in the *ceh-60* mutant (1% false discovery rate [FDR], Figures 4 and S4B). Furthermore, genes that were up-regulated in *ceh-60* day 1 adults tend to remain elevated later in adulthood (62%), while down-regulated genes were less likely to remain depressed (22%, Figure S4C), possibly because some of these genes are indirectly controlled by CEH-60 and subject to compensatory regulation.

The observed up- and down-regulation of gene expression in *ceh-60* mutants suggested that CEH-60/PBX may function as either a transcriptional repressor or activator in *C. elegans*, respectively, a phenomena previously attributed to different *PBX* isoforms or to alterations in PBX activity in response to cellular signaling events in mammals (Saleh et al., 2000; Asahara et al., 1999). To determine whether the genes mis-expressed in the *ceh-60* mutant are direct transcriptional targets of CEH-60, I performed chromatin immunoprecipitations of the endogenously tagged 3xHA-mCherry::CEH-60 protein using two different anti-HA antibodies and identified CEH-60-bound regions of the genome by sequencing (chromatin immunoprecipitation sequencing [ChIP-seq]). A strong enrichment for CEH-60 was observed at the transcriptional start sites (TSS) of genes that were transcriptionally up-regulated in the *ceh-60* mutant, indicating that CEH-60 functions broadly as a transcriptional repressor (Figure 4A). In contrast, the majority of genes transcriptionally down-regulated in the *ceh-60* mutant were not directly bound by CEH-60, suggesting that most of these regulatory effects are indirect. Nevertheless, a small set of down-regulated genes, including the *vit* genes, were strongly bound by CEH-60 (Figure 4A inset). Thus, CEH-60 functions as a transcriptional activator in the intestine where the *vit* genes are exclusively expressed and as a repressor in the intestine or in a different cell type (i.e., sensory neurons).

To define the tissue specificity of CEH-60 repressive activity, I determined whether the up- or down-regulated genes in the *ceh-60* mutant were enriched for a particular cell type using previously defined gene lists (Kaletsky et al., 2016; Pauli et al., 2006). Surprisingly, up-regulated genes are highly enriched in the intestine, suggesting that CEH-60 also acts as a transcriptional repressor in intestinal nuclei (Figure 4B). Consistently, the promoters of intestinal genes are robustly bound by CEH-60 (Figure 4C). In contrast, CEH-60 does not directly or indirectly regulate a large number of neuronal genes, suggesting that its neuronal function may be limited to a specific neuronal cell type or to the regulation of a small set of genes. In support of these enrichment analyses, hyper-activation of the CEH-60-repressed intestinal genes in the *ceh-60* mutant background, which can be reproducibly measured by RT-qPCR, was rescued by ectopic expression of *ceh-60* in the intestine, but not in the neurons (Figures S4D and S4E). Lastly, germline genes, which were not directly regulated by CEH-60 (Figure 4C), were down-regulated in the *ceh-60* mutant, likely due to the severe down-regulation of yolk delivered to the germline. Together, these data demonstrate that CEH-60, which is translated from a single mRNA isoform, performs dual roles within intestinal cell nuclei as both a transcriptional activator and repressor.

CEH-60/PBX Regulates Gene Expression in Concert with UNC-62/MEIS

PBC homeodomain transcription factors are known to cooperatively bind DNA in heterodimeric or trimeric complexes with other

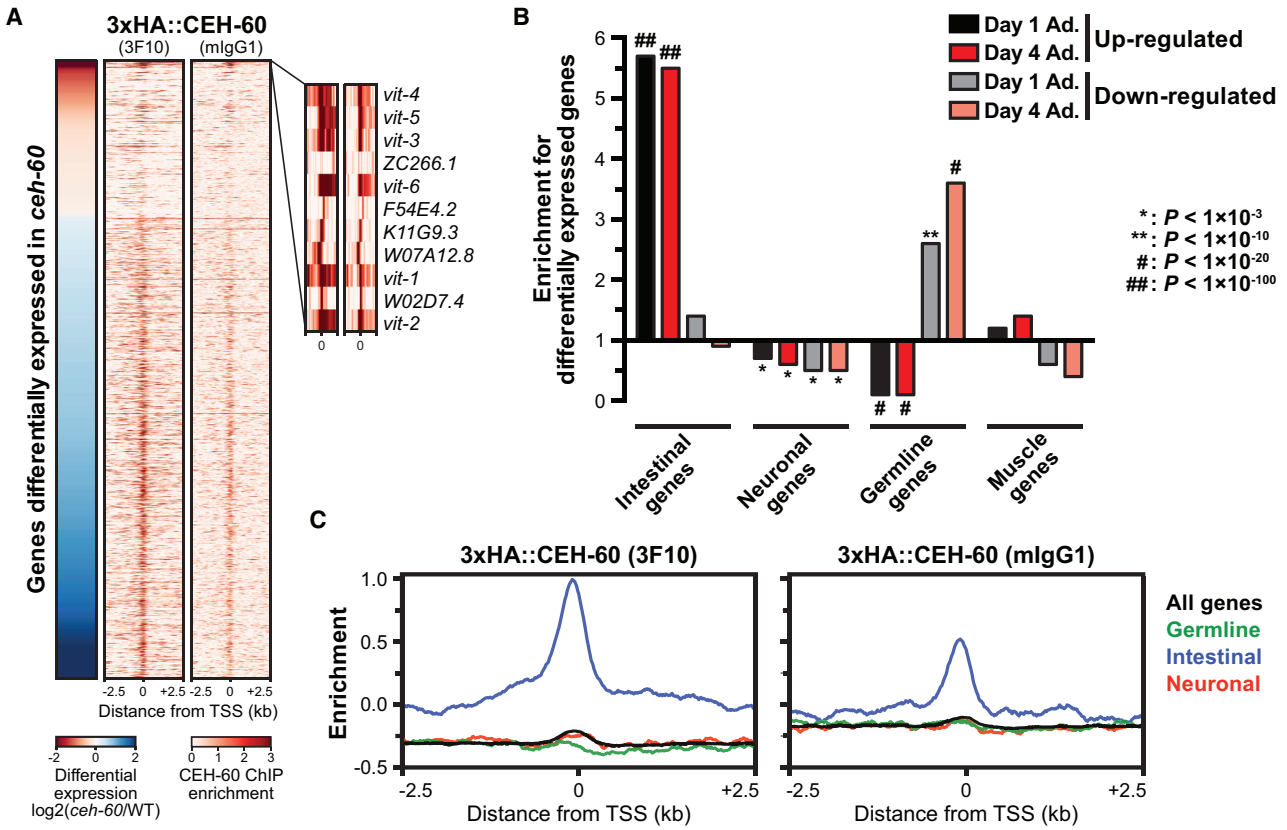

Figure 4. Dual Functionality of CEH-60 in Intestinal Gene Regulation

(A) Heatmap of 3xHA-mCherry::CEH-60 ChIP-seq signal (enrichment relative to input) using different anti-HA antibodies at the transcriptional start sites (TSS) of genes differentially expressed in *ceh-60(ok1485)* day 1 adult animals (1,928 genes). The enlarged inset panel shows a subset of genes that are directly activated by CEH-60.

(B) Enrichment for differential expression within the indicted gene classes (observed ÷ expected, hypergeometric p values reported).

(C) The average CEH-60 enrichment (ChIP-seq signal) at the TSS of the indicated gene classes.

See also Figure S4.

homeodomain proteins, particularly MEIS and Hox (Mann and Chan, 1996). In *C. elegans*, MEIS is encoded by *unc-62*, which is known to function in non-intestinal tissues with two additional PBC proteins, CEH-20 and CEH-40 (Jiang et al., 2009; Yang et al., 2005; Van Auken et al., 2002), and has been implicated in regulating developmental and longevity pathways (Van Nostrand et al., 2013). Although *ceh-60* is predicted to encode a PBC homeodomain protein, its genetic or biochemical interaction with MEIS has not been demonstrated.

To determine whether CEH-60/PBX functions in concert with UNC-62/MEIS, I performed ChIP-seq experiments using a strain that carries the endogenously tagged 3xHA-mCherry::CEH-60 allele along with a low-copy-number UNC-62(7a)::GFP transgene, which expresses an isoform of *unc-62* that is enriched in the intestine (Van Nostrand et al., 2013). The UNC-62(7a)::GFP protein co-localized with CEH-60 at the promoters of the *vit-3* and *vit-4* genes (Figure 5A). Consistently, intestine-specific knockdown of *unc-62* reduced *vit* gene expression as well as enhanced the *vit* expression defects of the *ceh-60* mutant without altering the expression of other known regulators of vitellogenesis (Figure 5B) (Goszczynski et al., 2016; Van Nostrand et al., 2013; Zhang et al., 2013). Furthermore, intestinal knockdown of *unc-62* phenocopied the *ceh-60* mutant defects in fat allocation and longevity (Figures S5A–S5E), supporting the premise that these proteins function together. Together, these data indicate that CEH-60 is a functional ortholog of mammalian PBX proteins that functions with UNC-62/MEIS to regulate vitellogenesis and lifespan, thereby establishing a previously unappreciated role for PBX in lipid metabolism and aging.

To expand on these observations, I determined CEH-60 and UNC-62(7a) enrichment at the TSS of all the genes mis-expressed in *ceh-60* mutants. Both transcription factors were enriched at the promoters of most of the CEH-60-repressed genes (Figure 5C). Interestingly, an identical analysis of an UNC-62 ChIP-seq dataset generated by the modENCODE consortium (Celniker et al., 2009) revealed that UNC-62 was present at most CEH-60-repressed genes at adulthood, as expected, but not at the L3 larval stage (Figure 5C). Consistently, inspection of all the UNC-62 ChIP-seq peaks, using either the UNC-62(7a) or the modENCODE datasets, revealed that a large number of UNC-62 binding sites were co-bound by CEH-60 at adulthood (UNC-62(7a), 99%; modENCODE UNC-62, 87%). However, at the L3 stage when CEH-60 is absent (Figure 2B), UNC-62 occupied significantly fewer regions that were bound by CEH-60 at

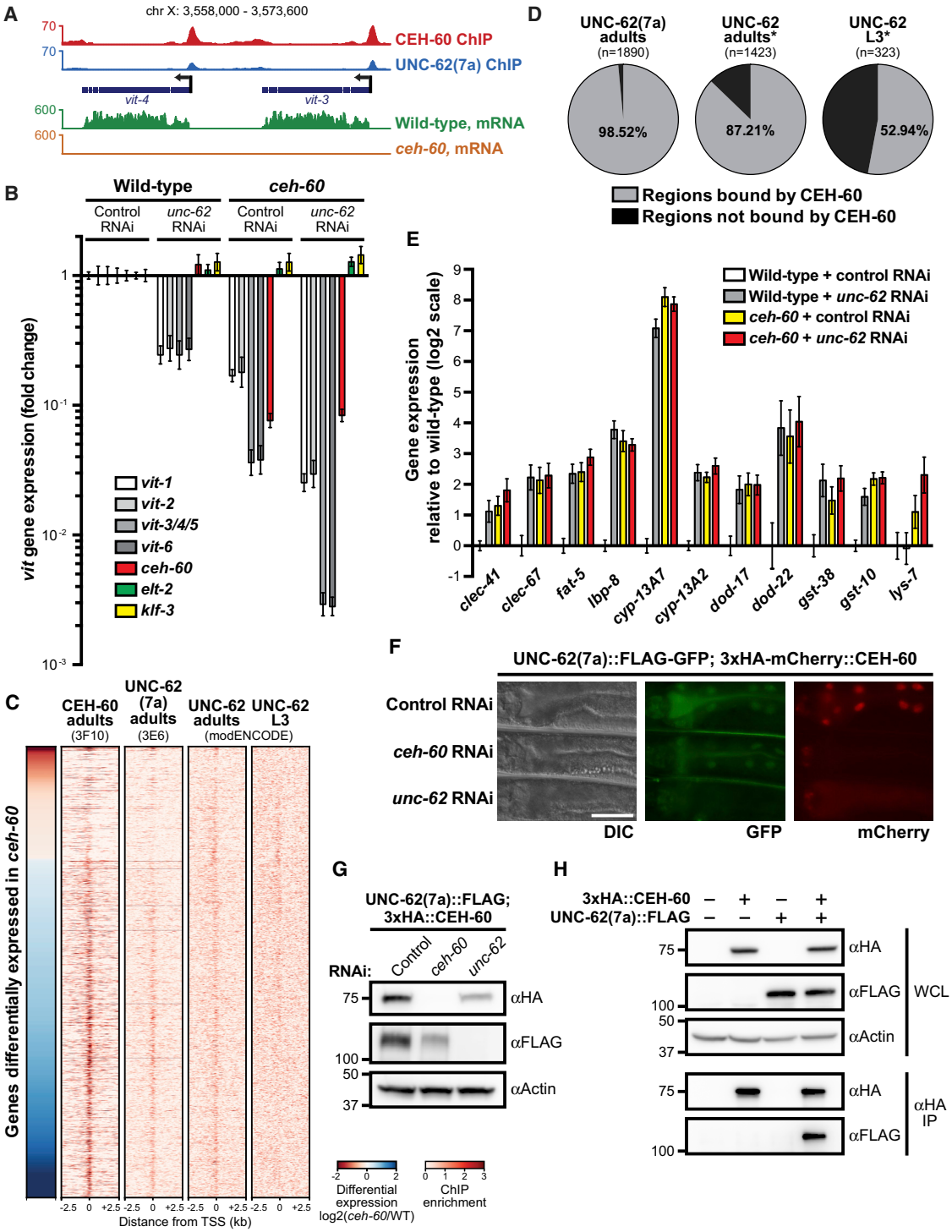

Figure 5. CEH-60/PBX Collaborates with UNC-62/MEIS to Control Intestinal Gene Expression

(A) Browser screenshot of CEH-60 and UNC-62 isoform 7a ChIP-seq signal at the *vit-3/4* locus, as well as normalized mRNA-seq reads (day 1 adults).

(B) RT-qPCR analysis of *vit* gene expression in MGH171 or DLS375 (intestinal-specific RNAi strains) subjected to control or *unc-62* RNAi. Data are plotted relative to MGH171 exposed to control RNAi as the mean +/− SEM.

(C) ChIP-seq signal at the TSS of *ceh-60(ok1485)* differentially expressed genes as in Figure 4A. The modENCODE UNC-62 ChIP-seq data were generated using the OP600 strain, which expresses all *unc-62* isoforms (Van Nostrand et al., 2013).

(D) Overlap between CEH-60 and UNC-62 ChIP-seq peaks after removal of HOT regions (*modENCODE data; n, number UNC-62 peaks).

(E) RT-qPCR analysis of gene expression (mean +/− SEM) at CEH-60-repressed genes for the strains in (B).

(legend continued on next page)

adulthood (53%, Figure 5D). It is possible that CEH-60 expression and heterodimerization with UNC-62 at the L4 stages helps to define and strengthen UNC-62 binding sites throughout the genome as the animal transitions into adulthood.

Co-occupation of CEH-60 and UNC-62 at the promoters of CEH-60-repressed genes suggests that these factors may heterodimerize to exert their effects at these targets, as I observed at the CEH-60-activated loci (i.e., *vit* genes). Indeed, loss of either *ceh-60* or *unc-62* in intestinal cells resulted in a similar up-regulation of gene expression at these normally repressed loci (Figure 5E). While it is feasible that both UNC-62 and CEH-60 proteins are individually required to recruit repressive factors, it is also possible that they stabilize or promote the subcellular localization of each other when simultaneously expressed in the cell (Rieckhof et al., 1997). To test this hypothesis, I examined the expression and localization of UNC-62::GFP or mCherry::CEH-60 in intestinal cells after inactivation of *ceh-60* or *unc-62*, respectively. While UNC-62::GFP expression and localization remained unchanged after loss of *ceh-60*, knockdown of *unc-62* resulted in a loss of mCherry::CEH-60 nuclear localization without dramatically altering overall protein levels (Figures 5F, 5G, S5F, and S5G), suggesting that CEH-60 and UNC-62 form a complex in the nucleus. In support of this hypothesis, immunoprecipitation of CEH-60 from whole-animal lysates resulted in co-purification of UNC-62 (Figure 5H), thereby confirming that the proteins form a complex. Together, these data demonstrate that expression of UNC-62/MEIS is necessary to retain CEH-60/PBX in the nucleus where the heterodimer functions as both an activator and repressor of gene expression.

Innate Immunity Genes Are Repressed by the CEH-60:UNC-62 Heterodimer

My genomic analyses revealed widespread repression of gene expression by the CEH-60:UNC-62 complex, suggesting that the heterodimer may restrict energy-demanding cellular processes in order to redirect resources into reproduction as the animal transitions into an adult. To investigate which pathways are repressed by CEH-60, I performed a Gene Ontology (GO) enrichment analysis on the genes mis-expressed in the *ceh-60* mutant. Expectedly, genes involved in fatty acid metabolism were strongly enriched among the differentially expressed genes, which is due, at least in part, to the accumulation of intestinal lipids that results from down-regulation of the vitellogenin (Figure 6A). Surprisingly, genes involved in innate immunity, defense against bacterial pathogens, and the oxidative stress response comprised the three most enriched categories. Differential expression of these ''defense'' genes (a composite of innate immunity and bacterial defense genes) was well correlated in the *ceh-60* and *unc-62* mutants (R^2 = 0.466, Figure 6B) (Van Nostrand et al., 2013). Moreover, the promoters of the differentially expressed defense genes were more strongly bound by CEH-60 and UNC-62(7a) than the average differentially expressed gene promoter, suggesting that they contain strong or multiple binding sites for the heterodimer (Figure 6C). Together, these data indicate that many defense-related genes are directly bound and repressed by the CEH-60:UNC-62 complex in wild-type adult animals. This phenomenon was exemplified at the *irg-4* locus (Figure 6D), which encodes a pathogen-induced immune effector containing a CUB-like domain that is required for survival during *Pseudomonas aeruginosa* infection (Shapira et al., 2006).

While elevated expression of innate immunity genes is likely important during larval development, maintaining their expression during reproduction may be energetically expensive. Basal expression of immunity genes is repressed by CEH-60:UNC-62 at adulthood; however, whether the heterodimer also represses immune genes during infection is unclear. To test this empirically, I challenged adult animals with the pathogenic bacterial strain *Pseudomonas aeruginosa* PA14 and analyzed gene expression by RT-qPCR (Tan et al., 1999). Importantly, both basal and pathogen-induced expression of two known immunity genes, *irg-4* and *clec-67*, was elevated in the *ceh-60* mutant (Figures 6E and S6A). Since inactivation of *ceh-60* results in hyper-activation of defense genes in response to pathogen, I performed longitudinal survival assays to determine whether *ceh-60* mutants display enhanced resistance to *Pseudomonas*. Loss of *ceh-60* resulted in a modest, but reproducible, increase in PA14 resistance (Figure 6F). Together, these results demonstrate that CEH-60 represses the innate immune response during adulthood, which may help to promote energy allocation into the reproductive process.

CEH-60 Associates with PQM-1 to Repress Gene Expression

Expression of CEH-60 at adulthood reconfigures the physiology of the organism to support reproduction while restricting longevity and stress responses; however, the transcriptional regulator(s) that function in concert with CEH-60:UNC-62 remain unclear. Most transcription factors bind specific, evolutionarily conserved consensus sequences within the promoters of their target genes, as has been demonstrated experimentally in *C. elegans* using ChIP-seq (Araya et al., 2014). For example, the mammalian PBX:MEIS heterodimer recognizes the TGATTGAC consensus sequence (Knoepfler and Kamps, 1997), and correspondingly, UNC-62 associates with the same binding motif in the worm (Van Nostrand et al., 2013). Using the MEME-ChIP motif discovery algorithm (Machanick and Bailey, 2011), I found strong enrichment for this PBX consensus element in regions bound by CEH-60, further substantiating its association with UNC-62/MEIS (Figures 7A and 7B). Surprisingly, CEH-60 binding sites were also enriched for a GATA-like sequence (TGATAAG) that is positioned directly adjacent to the PBX consensus element, and which was present in the promoters of both CEH-60-repressed and CEH-60-activated

(F) Representative fluorescence images of intestinal mCherry::CEH-60 and UNC-62(7a):GFP expression and localization after knockdown of *ceh-60* or *unc-62* using a strain carrying the *glo-4(ok623)* mutation. Scale bar, 100 μm.

(G) Western blot showing CEH-60 and UNC-62(7a) protein levels for the animals described in (F). Actin is shown as a loading control.

(H) Western blots detecting CEH-60, UNC-62(7a), or actin in whole-cell lysates (WCL) or anti-HA immunoprecipitations. The gel lanes correspond to protein isolated from wild-type, DLS395, SD1890, and DLS396 strains (left to right).

See also Figure S5.

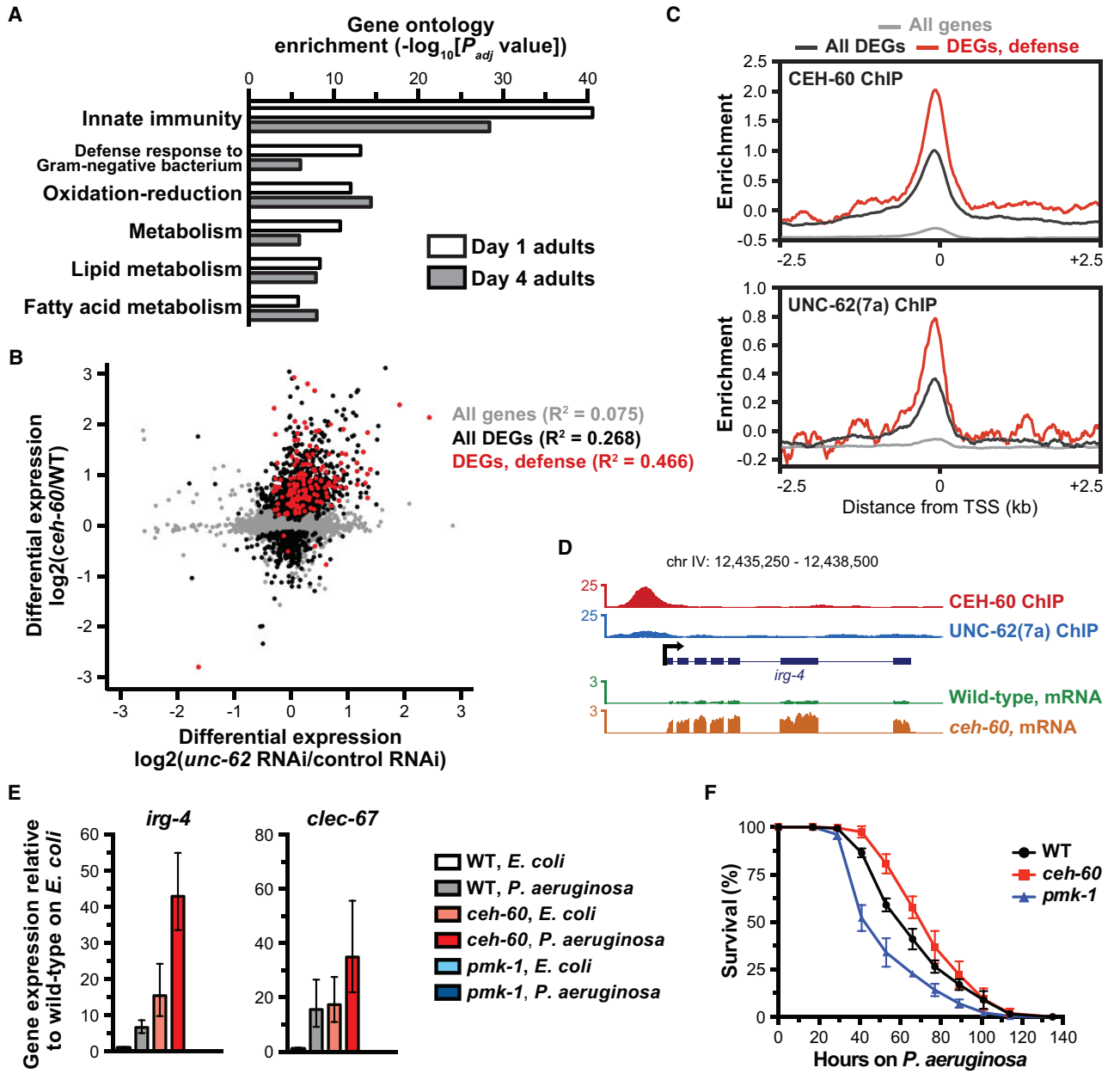

Figure 6. Innate Immunity Pathways Are Coordinated by the CEH-60:UNC-62 Transcriptional Complex

(A) Gene Ontology enrichment analysis of genes differentially expressed in the *ceh-60(ok1485)* mutant. The top six categories are reported as the $-\log_{10}$ transformation of the Benjamini-Hochberg corrected p value.

(B) A scatterplot of differential gene expression in *ceh-60(ok1485)* versus *unc-62* RNAi for the indicated gene classes (DEGs, differentially expressed genes; defense, genes annotated to function to innate immunity or pathogen defense). The R^2 coefficient of determination values are given for each class.

(C) The average CEH-60 and UNC-62(7a) ChIP-seq signal at the indicated gene classes.

(D) Browser screenshot showing CEH-60 and UNC-62(7a) ChIP-seq signal, as well as wild-type and *ceh-60(ok1485)* normalized mRNA-seq reads, at the *irg-4* locus.

(E) RT-qPCR analysis of *irg-4* and *clec-67* gene expression (mean +/− SEM) in wild-type, *ceh-60(ok1485)*, and *pmk-1(km25)* animals exposed to *E. coli* OP50 or *P. aeruginosa* PA14. *pmk-1* encodes a p38 MAP kinase ortholog that is required for pathogen defense.

(F) Longitudinal survival assay (mean ± SD) of the strains in (E) on *P. aeruginosa* PA14.

See also Figure S6.

genes (Figures 7A, 7B, and S7A). These data suggest that CEH-60 may associate with or compete against a GATA-like transcription factor for access to these motifs.

To expand on these observations and place CEH-60 within a larger transcriptional network, I determined the ChIP enrichment at the promoters of CEH-60-regulated genes for each of

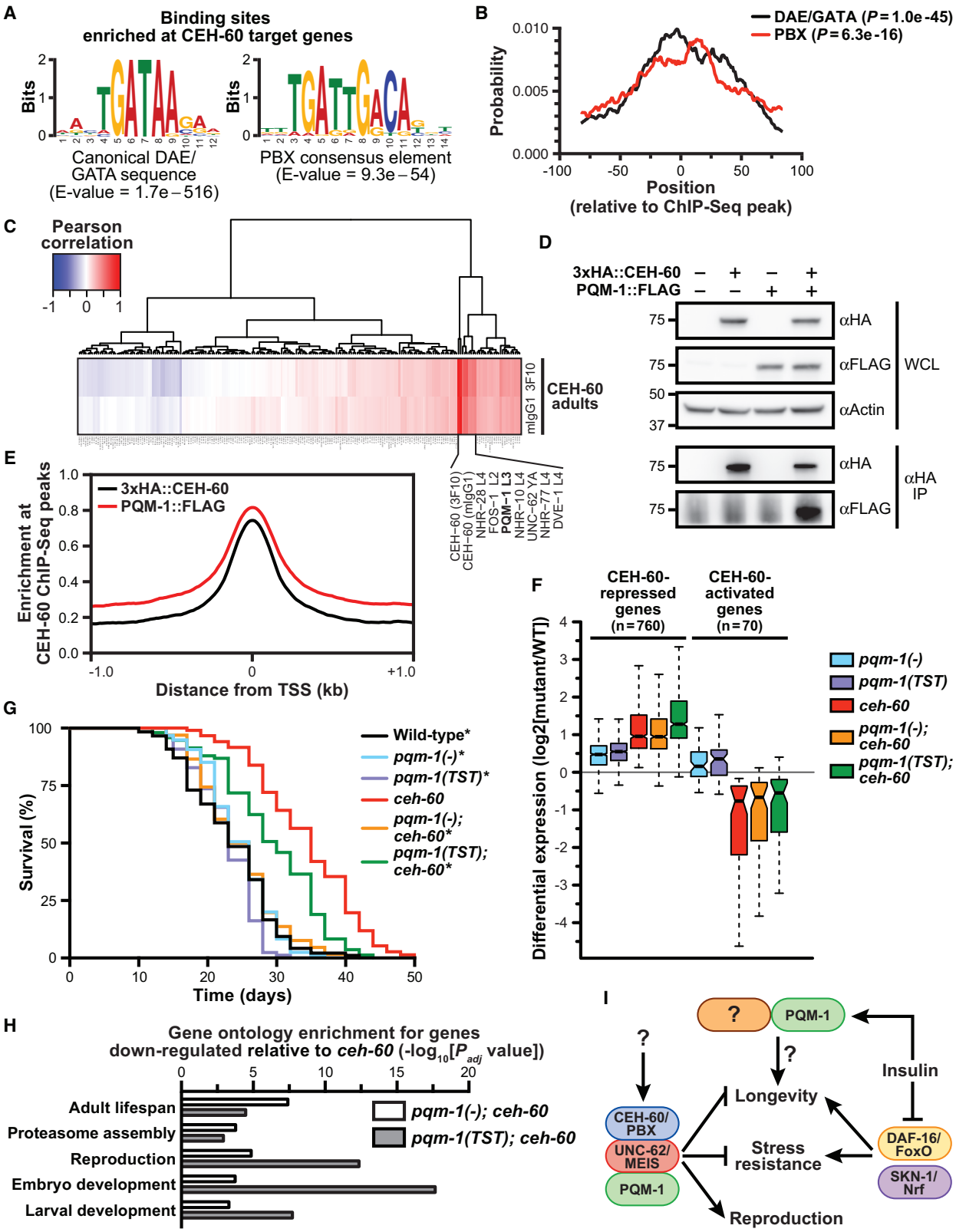

Figure 7. CEH-60 Associates with PQM-1 to Repress Gene Expression

(A) Enriched motifs, and their corresponding E-values, at CEH-60 target genes.

(B) The motif positional probability at those genes analyzed in (A).

(legend continued on next page)

the ~100 transcriptional regulators that have been previously profiled using ChIP-seq by the modENCODE consortium (210 datasets) (Celniker et al., 2009). Hierarchal clustering of the Pearson correlations between the CEH-60 dataset and all other datasets revealed that a small set of proteins have similar binding patterns to CEH-60, including UNC-62 and the C2H2 zinc-finger transcription factor PQM-1 (L3 data, Figure 7C). A similar co-association pattern has been previously observed between UNC-62 and PQM-1 (Araya et al., 2014). In response to changes in insulin signaling, PQM-1 and DAF-16/FoxO function antagonistically, with PQM-1 directly activating expression of developmental genes by binding to the DAF-16-associated element (DAE) during wild-type insulin conditions (DAF-16 cytoplasmic), while reduced insulin signaling prompts DAF-16 nuclear localization (PQM-1 cytoplasmic) and up-regulation of stress-response genes via the DAF-16-binding element (Tepper et al., 2013). The DAE is also enriched at these DAF-16-dependent stress-response genes; however, PQM-1's role at these genes is poorly understood. Consistent with my observation that CEH-60 and PQM-1 occupy overlapping sites in the genome, the GATA-like motif enriched in CEH-60 binding sites is indeed the DAE consensus sequence (Figure 7A), suggesting that the two factors may function together at the DAE motifs in the promoters of stress-response genes.

To further explore the relationship between PQM-1 and CEH-60, I first assessed whether the two factors form a multimeric complex. Indeed, immunoprecipitation of HA::CEH-60 or PQM-1::FLAG from animal lysates resulted in co-purification of PQM-1::FLAG or HA::CEH-60, respectively (Figures 7D and S7B). Moreover, PQM-1 binds to the same regions of the genome as CEH-60 in adult animals when both transcription factors are expressed (Figure 7E). Importantly, loss of *pqm-1* or *ceh-60* only had a modest detrimental effect on CEH-60 or PQM-1 binding to chromatin, respectively, indicating that each transcription factor is capable of associating with their respective binding motif independently of each other (Figures S7C and S7D).

Together, my results suggest that PQM-1 associates with CEH-60:UNC-62 at the GATA-like DAE motif to control gene expression; however, whether PQM-1 functions with or against CEH-60 is unclear. To address this, I performed mRNA-seq on the *pqm-1(-)* null mutant, as well as the *pqm-1(-); ceh-60* double mutant, and determined whether the CEH-60 target genes are differentially expressed in these mutant backgrounds. Indeed, loss of *pqm-1* resulted in up-regulation of the CEH-60-repressed genes (i.e., stress-response genes); however, deletion of *pqm-1* failed to further enhance the transcriptional defects conferred by loss of *ceh-60* (Figure 7F). The C terminus of PQM-1 contains a putative AKT/SGK-1 phosphorylation site that may control its transcriptional activity or subcellular localization (Dowen et al., 2016; Tepper et al., 2013). Using CRISPR/Cas9, I generated a *pqm-1* mutant that lacks these residues (T266A/S267A/T268A) and assessed its transcriptional activity by mRNA-seq. Remarkably, CEH-60 targets are also up-regulated in this background, suggesting that phosphorylation of PQM-1 may be required for its repressive activity (Figure 7F). Although repression of CEH-60 target genes required *pqm-1*, an identical analysis of CEH-60-activated genes revealed *pqm-1* is dispensable for this activity. Importantly, these transcriptional defects in the *pqm-1* mutants were not simply a consequence of *ceh-60* down-regulation; in fact, both factors normally bind to each other's promoters to repress gene expression (Figures S7E–S7G). An identical analysis of genes that are directly repressed by PQM-1 revealed that CEH-60 also functions at these genes as a transcriptional co-repressor (Figure S7H). Together, these results establish a cooperative role for PQM-1 in repression of CEH-60 target genes; however, not all of the genes mis-regulated upon loss of *ceh-60* showed a corresponding *pqm-1* dependence (Figure S7I), indicating that PQM-1 may function differently within the context of individual promoters.

Despite the observation that PQM-1 functions antagonistically to the pro-longevity factor DAF-16, the extended lifespan of *daf-2* mutants requires both *pqm-1* and *daf-16* (Tepper et al., 2013). Consistent with this observation, the long-lived phenotype of the *ceh-60* mutant was suppressed by either complete loss of *pqm-1* or by mutation of the AKT/SGK-1 phosphorylation sites (Figure 7G). These results were surprising in light of the collaborative role for CEH-60 and PQM-1 in repression of stress-response and/or longevity genes. To gain additional insight into this genetic interaction, I performed a GO enrichment analysis on those genes down-regulated in the *pqm-1; ceh-60* double mutant relative to the *ceh-60* mutant, which revealed that PQM-1 positively regulates, either directly or indirectly, an additional set of longevity genes (Figure 7H). Taken together, these results suggest that PQM-1 represses stress-response genes in collaboration with CEH-60:UNC-62, while simultaneously shaping other transcriptional networks to positively regulate longevity (Figure 7I).

DISCUSSION

Here, I demonstrate that CEH-60/PBX is a linchpin developmental regulator of intestinal resources that mediates the balance between reproduction and longevity to maintain organismal

(C) Hierarchical clustering of the ChIP-seq signal proximal to *ceh-60(ok1485)* differentially expressed genes (+/− 2.5 kb of TSS) based on the Pearson correlation for the indicated modENCODE datasets.
(D) Western blots detecting CEH-60, PQM-1, and actin in whole-cell lysates (WCL) or anti-HA immunoprecipitations. The gel lanes correspond to protein isolated from wild-type, DLS395, OP201, and DLS448 strains (left to right).
(E) The average ChIP-seq signal for the indicated samples at CEH-60 peaks after removal of HOT regions.
(F) Differential expression of high confidence CEH-60 target genes in the *pqm-1(ok485)*, *pqm-1(rhd90[TST/AAA])*, *ceh-60(ok1485)*, *pqm-1(ok485); ceh-60*, and *pqm-1(rhd90); ceh-60* mutants.
(G) Longitudinal lifespan assay of the strains described in (F). All survival curves are significantly different compared with the *ceh-60* curve ($p < 0.0001$).
(H) A Gene Ontology enrichment analysis of genes differentially expressed in the *pqm-1(ok485)*; *ceh-60(ok1485)* and *pqm-1(rhd90[TST/AAA]); ceh-60(ok1485)* mutants relative to *ceh-60(ok1485)*.
(I) A model of CEH-60, UNC-62, and PQM-1 function in intestinal gene regulation.
See also Figure S7.

homeostasis. Intestinal expression of *ceh-60* at the mid-late L4 stage, which corresponds with maturation of the germline, supports reproduction by directly activating vitellogenin gene expression. CEH-60 functions in concert with UNC-62/MEIS, which is expressed throughout development, in a heterodimeric complex to activate genes involved in reproduction (i.e., vitellogenin) while simultaneously repressing longevity and stress genes (Figure 7I). Moreover, my work revealed that CEH-60 functions with PQM-1 to directly repress numerous stress-responsive genes, which are normally activated by DAF-16/FoxO and/or SKN-1/Nrf, thereby establishing CEH-60 as a new component of this complex transcriptional network that responds to a variety of developmental and environmental inputs.

The *ceh-60* and *unc-62* mutants display many phenotypic similarities, which are at least partially due to the fact that UNC-62 is responsible for retaining CEH-60 in the nucleus to maintain heterodimerization. Induction of *ceh-60* expression at adulthood is likely to impart cooperative binding-site specificity and temporal gene regulation that is absent when only UNC-62 is present (e.g., L3 animals), as has been described for their orthologs EXD and HTH during fly development (Rieckhof et al., 1997; Mann and Chan, 1996). Surprisingly, gene activation and repression by the CEH-60:UNC-62 complex occurs simultaneously in the nucleus, which has yet to be described for PBC homeodomain proteins and is an unusual feature among transcription factors. It is possible that the heterodimer functions in conjunction with different cofactors that are defined by the local sequence contexts within the target gene promoters (Pan and Courey, 1992). Alternatively, post-translational modification of CEH-60 or UNC-62 may locally define the activity of the complex within the genome (Huang et al., 2005; Saleh et al., 2000).

CEH-60 and UNC-62 are direct transcriptional repressors of longevity, a unique biological function among transcription factors. Notably, loss of the ETS-4 transcription factor dramatically extends lifespan; however, this result is explained by the finding that these mutants fail to express *ceh-60* (Thyagarajan et al., 2010). It is interesting to speculate whether PBX and MEIS may similarly reconfigure cellular homeostasis in mammals to restrict organismal lifespan. In the worm, mutation of *ceh-60* or *unc-62* extends lifespan without dramatically altering brood size, although the progeny do show compromised fitness during L1 starvation because of the maternal vitellogenesis defects (Van Rompay et al., 2015). Notably, the *rme-2; ceh-60* double mutant is sterile (data not shown), indicating that the *ceh-60* mutation does not suppress the fertility defects associated with loss of vitellogenesis. Rather, other transcriptional activators of vitellogenin expression, such as the intestinal GATA transcription factor ELT-2, are likely functioning in the absence of *ceh-60* to produce a sufficient amount of vitellogenin to support viability (Goszczynski et al., 2016). It is likely that the dramatically reduced level of yolk in the *ceh-60* mutant is sufficient to support the embryonic cell divisions of the progeny, yet unable to sustain prolonged L1 survival in the absence of food, thereby putting these animals at an evolutionary disadvantage in the wild. Nonetheless, the remarkable phenotypic duality displayed by the *ceh-60* mutant is a striking contradiction of the disposable soma theory, which argues that an organism's reproductive fitness is inversely related to its somatic longevity because limited resources must be appropriately allocated between either somatic or germline tissues.

Loss of *ceh-60* or *unc-62* extends lifespan via the pro-longevity transcription factor DAF-16 (Van Nostrand et al., 2013). While I did not observe robust nuclear accumulation of DAF-16 protein in the *ceh-60* mutant, this translocation event is not absolutely necessary for the *daf-16*-dependent lifespan extension of other mutants (Arum and Johnson, 2007; Henderson and Johnson, 2001). Similarly, the *ceh-60* mutant fails to accumulate SKN-1 in the nucleus, yet *skn-1* is required for the lifespan extension. While *daf-16* and *skn-1* are both required for the extended lifespan of the *ceh-60* mutant, possibly because they regulate some overlapping transcriptional targets that promote longevity (Tullet et al., 2008), these proteins did not participate in vitellogenin regulation in the *ceh-60* mutant, demonstrating that vitellogenesis and longevity are uncoupled in this genetic background. In support of this observation, the *ceh-60* mutation enhanced the lifespan of the *rme-2* mutant, which is completely defective in vitellogenesis. Thus, CEH-60 normally represses longevity genes to promote aging, a process that occurs independently of its role in vitellogenesis. In addition, my results argue that some of the transcriptional targets of DAF-16 and SKN-1 are repressed, either directly or indirectly, by CEH-60 to restrict longevity, and when *ceh-60* is lost, excess accumulation of DAF-16/SKN-1 protein in the nucleus is not necessary to extend lifespan (Figure 3F).

Increased longevity is known to correlate with enhanced resistance to a variety of abiotic or biotic stresses, but the molecular basis for this physiological relationship is not well understood. For example, reduced insulin signaling enhances longevity on non-pathogenic food sources, as well as survival on the bacterial pathogen *Pseudomonas aeruginosa*, requiring *daf-16* and *skn-1* (Papp et al., 2012; Garsin et al., 2003). Here, I have identified CEH-60 as a global repressor of pathogen response genes, which suggests that CEH-60 may be inhibited or displaced during the transcriptional response to infection. Notably, this function may be evolutionarily conserved, as overexpression of PBX3 results in widespread mis-expression of immunity genes in hepatocytes (Han et al., 2015). This work establishes CEH-60 as a central regulator of the pathogen response and suggests that the pathways that respond to infection, including insulin and PMK-1/p38 MAPK signaling, may do so in part by dynamically altering the transcriptional activity of CEH-60.

Using genomic and transcriptomic approaches, I found that the CEH-60:UNC-62 heterodimer associates with PQM-1 at the GATA-like DAE motif to exert widespread gene repression in the intestine. Most of these sites are bound by PQM-1 at the L3 stage (data not shown), suggesting that PQM-1 may recruit or stabilize CEH-60:UNC-62 at these genes later in development; however, how PQM-1 regulates its target genes during larval development remains unclear. Notably, the promoters of CEH-60-activated genes, including the *vit* genes, also contain the DAE motif yet do not require *pqm-1* for their expression, suggesting that additional factors may be present at these promoters that direct the activity of CEH-60:UNC-62:PQM-1.

I propose that during normal growth conditions, the association of CEH-60 with PQM-1 late in larval development promotes the transition from a moderate stress-resistant state, largely mediated by the basal activities of DAF-16 and SKN-1, toward a reproductive state (Figure 7I). Upon reduced insulin signaling, however, dephosphorylation of DAF-16 and SKN-1 triggers their

entry into the nucleus while PQM-1 exits, which may diminish the repressive activity of CEH-60 at stress-responsive genes and facilitate activation of these genes by DAF-16/SKN-1. Phosphorylation is likely to play a key role in positively regulating PQM-1 activity, which is supported by the observation that the *pqm-1(TST/AAA)* mutant phenocopies the transcriptional defects displayed by the *pqm-1* and *ceh-60* null mutants at CEH-60-repressed genes. It is possible that phosphorylation of PQM-1 controls its nuclear localization or promotes its ability to associate with CEH-60; however, a rigorous biochemical analysis of the phosphorylation status of PQM-1 in response to different cellular perturbations, including modified insulin signaling, will be essential to gain mechanistic insight into how PQM-1 is post-translationally regulated.

Proper allocation of resources between somatic and germline functions based on developmental and environmental information is fundamentally important for the survival of a species, yet the underlying regulators that mediate this trade-off remain poorly understood. I have uncovered an unexpected and significant role for the largely uncharacterized CEH-60/PBX transcription factor in supporting reproduction and suppressing somatic longevity and stress responses. As a previously unappreciated governor of cellular resources, it will be important to understand whether CEH-60 transcriptional activity is dictated by cellular signaling events. A likely candidate is the insulin signaling pathway, which may be responsible for controlling the expression, subcellular localization, cofactor interactions, transcriptional activity, or binding affinity of CEH-60. This work establishes a robust platform to further define the molecular basis of how the evolutionarily conserved CEH-60 protein functions in lipid metabolism, stress responses, and the natural aging process in humans.

STAR★METHODS

Detailed methods are provided in the online version of this paper and include the following:

- KEY RESOURCES TABLE
- CONTACT FOR REAGENT AND RESOURCE SHARING
- EXPERIMENTAL MODEL AND SUBJECT DETAILS
- METHOD DETAILS
  - Generation of Transgenic Strains
  - Imaging of Transgenic Animals
  - RNAi Experiments
  - Oil Red O Staining
  - Image Analysis
  - Quantitative PCR
  - Western Blot Analyses
  - Lifespan and Brood Size Assays
  - Pseudomonas aeruginosa Assays
  - Chromatin Immunoprecipitation
  - Library Preparation
  - Sequencing Read Mapping and Downstream Processing
  - Genomic Data Correlations and Analyses
  - Gene Ontology Enrichment
  - Enriched Motif Analysis
- QUANTIFICATION AND STATISTICAL ANALYSIS
- DATA AND SOFTWARE AVAILABILITY

SUPPLEMENTAL INFORMATION

Supplemental Information can be found online at https://doi.org/10.1016/j.devcel.2019.03.002.

ACKNOWLEDGMENTS

Some of the strains used in this work were provided by the Caenorhabditis Genetics Center (P40 OD010440). The P*irg-4*::*GFP* reporter and *P. aeruginosa* PA14 were generously provided by Read Pukkila-Worley. I would like to thank Read Pukkila-Worley, Jill Dowen, Shawn Ahmed, Dan McKay, and Bob Duronio for critical reading of the manuscript. This work was funded by the Integrative Program for Biological and Genome Sciences, the Department of Biology, the UNC Lineberger Comprehensive Cancer Center, and the Department of Biochemistry and Biophysics at the University of North Carolina at Chapel Hill.

AUTHOR CONTRIBUTIONS

R.H.D. designed and performed the experiments, interpreted the results, and prepared the manuscript.

DECLARATION OF INTERESTS

The author declares no competing interests.

Received: April 30, 2018
Revised: November 26, 2018
Accepted: March 4, 2019
Published: April 4, 2019

REFERENCES

Arantes-Oliveira, N., Apfeld, J., Dillin, A., and Kenyon, C. (2002). Regulation of life-span by germ-line stem cells in *Caenorhabditis elegans*. Science *295*, 502–505.

Araya, C.L., Kawli, T., Kundaje, A., Jiang, L., Wu, B., Vafeados, D., Terrell, R., Weissdepp, P., Gevirtzman, L., Mace, D., et al. (2014). Regulatory analysis of the *C. elegans* genome with spatiotemporal resolution. Nature *512*, 400–405.

Arum, O., and Johnson, T.E. (2007). Reduced expression of the *Caenorhabditis elegans* p53 ortholog *cep-1* results in increased longevity. J. Gerontol. A Biol. Sci. Med. Sci. *62*, 951–959.

Asahara, H., Dutta, S., Kao, H.Y., Evans, R.M., and Montminy, M. (1999). Pbx-Hox heterodimers recruit coactivator-corepressor complexes in an isoform-specific manner. Mol. Cell. Biol. *19*, 8219–8225.

Bailey, T.L., and Machanick, P. (2012). Inferring direct DNA binding from ChIP-seq. Nucleic Acids Res. *40*, e128.

Baumeister, R., Schaffitzel, E., and Hertweck, M. (2006). Endocrine signaling in *Caenorhabditis elegans* controls stress response and longevity. J. Endocrinol. *190*, 191–202.

Bishop, N.A., and Guarente, L. (2007). Two neurons mediate diet-restriction-induced longevity in *C. elegans*. Nature *447*, 545–549.

Boyle, A.P., Araya, C.L., Brdlik, C., Cayting, P., Cheng, C., Cheng, Y., Gardner, K., Hillier, L.W., Janette, J., Jiang, L., et al. (2014). Comparative analysis of regulatory information and circuits across distant species. Nature *512*, 453–456.

Brenner, S. (1974). The genetics of *Caenorhabditis elegans*. Genetics *77*, 71–94.

Celniker, S.E., Dillon, L.A., Gerstein, M.B., Gunsalus, K.C., Henikoff, S., Karpen, G.H., Kellis, M., Lai, E.C., Lieb, J.D., MacAlpine, D.M., et al. (2009). Unlocking the secrets of the genome. Nature *459*, 927–930.

ENCODE Project Consortium (2012). An integrated encyclopedia of DNA elements in the human genome. Nature *489*, 57–74.

DePina, A.S., Iser, W.B., Park, S.S., Maudsley, S., Wilson, M.A., and Wolkow, C.A. (2011). Regulation of *Caenorhabditis elegans* vitellogenesis by DAF-2/IIS through separable transcriptional and posttranscriptional mechanisms. BMC Physiol. *11*, 11.

Dickinson, D.J., Ward, J.D., Reiner, D.J., and Goldstein, B. (2013). Engineering the *Caenorhabditis elegans* genome using Cas9-triggered homologous recombination. Nat. Methods *10*, 1028–1034.

Dobin, A., Davis, C.A., Schlesinger, F., Drenkow, J., Zaleski, C., Jha, S., Batut, P., Chaisson, M., and Gingeras, T.R. (2013). STAR: ultrafast universal RNA-seq aligner. Bioinformatics *29*, 15–21.

Dowen, R.H., Breen, P.C., Tullius, T., Conery, A.L., and Ruvkun, G. (2016). A microRNA program in the *C. elegans* hypodermis couples to intestinal mTORC2/PQM-1 signaling to modulate fat transport. Genes Dev. *30*, 1515–1528.

Frokjaer-Jensen, C., Davis, M.W., Hopkins, C.E., Newman, B.J., Thummel, J.M., Olesen, S.P., Grunnet, M., and Jorgensen, E.M. (2008). Single-copy insertion of transgenes in *Caenorhabditis elegans*. Nat. Genet. *40*, 1375–1383.

Garsin, D.A., Villanueva, J.M., Begun, J., Kim, D.H., Sifri, C.D., Calderwood, S.B., Ruvkun, G., and Ausubel, F.M. (2003). Long-lived *C. elegans daf-2* mutants are resistant to bacterial pathogens. Science *300*, 1921.

Gibson, D.G., Young, L., Chuang, R.Y., Venter, J.C., Hutchison, C.A., 3rd, and Smith, H.O. (2009). Enzymatic assembly of DNA molecules up to several hundred kilobases. Nat. Methods *6*, 343–345.

Goszczynski, B., Captan, A.M., Lancaster, B.R., McGhee, J.D., and Danielson, V.V. (2016). A 44 bp intestine-specific hermaphrodite-specific enhancer from the C. elegans vit-2 vitellogenin gene is directly regulated by ELT-2, MAB-3, FKH-9 and DAF-16 and indirectly regulated by the germline, by daf-2/insulin signaling and by the TGF-beta/Sma/Mab pathway. Dev. Biol. *413*, 112–127.

Grant, B., and Hirsh, D. (1999). Receptor-mediated endocytosis in the *Caenorhabditis elegans* oocyte. Mol. Biol. Cell *10*, 4311–4326.

Han, H.B., Du, Y.T., Zhao, W., Li, S., Chen, D.J., Zhang, J., Liu, J., Suo, Z.H., Bian, X.W., Xing, B.C., et al. (2015). PBX3 is targeted by multiple miRNAs and is essential for liver tumour-initiating cells. Nat. Commun. *6*, 8271.

Henderson, S.T., and Johnson, T.E. (2001). *daf-16* integrates developmental and environmental inputs to mediate aging in the nematode *Caenorhabditis elegans*. Curr. Biol. *11*, 1975–1980.

Huang da, W., Sherman, B.T., and Lempicki, R.A. (2009). Systematic and integrative analysis of large gene lists using DAVID bioinformatics resources. Nat. Protoc. *4*, 44–57.

Huang, H., Rastegar, M., Bodner, C., Goh, S.L., Rambaldi, I., and Featherstone, M. (2005). MEIS C termini harbor transcriptional activation domains that respond to cell signaling. J. Biol. Chem. *280*, 10119–10127.

Jiang, Y., Shi, H., and Liu, J. (2009). Two Hox cofactors, the Meis/Hth homolog UNC-62 and the Pbx/Exd homolog CEH-20, function together during *C. elegans* postembryonic mesodermal development. Dev. Biol. *334*, 535–546.

Kaletsky, R., Lakhina, V., Arey, R., Williams, A., Landis, J., Ashraf, J., and Murphy, C.T. (2016). The *C. elegans* adult neuronal IIS/FOXO transcriptome reveals adult phenotype regulators. Nature *529*, 92–96.

Kirkwood, T.B. (1977). Evolution of ageing. Nature *270*, 301–304.

Kirkwood, T.B., and Holliday, R. (1979). The evolution of ageing and longevity. Proc. R. Soc. Lond. B Biol. Sci. *205*, 531–546.

Knoepfler, P.S., and Kamps, M.P. (1997). The highest affinity DNA element bound by Pbx complexes in t(1;19) leukemic cells fails to mediate cooperative DNA-binding or cooperative transactivation by E2a-Pbx1 and class I Hox proteins - evidence for selective targetting of E2a-Pbx1 to a subset of Pbx-recognition elements. Oncogene *14*, 2521–2531.

Langmead, B., and Salzberg, S.L. (2012). Fast gapped-read alignment with Bowtie 2. Nat. Methods *9*, 357–359.

Li, H., Handsaker, B., Wysoker, A., Fennell, T., Ruan, J., Homer, N., Marth, G., Abecasis, G., and Durbin, R.; 1000 Genome Project Data Processing Subgroup (2009). The Sequence Alignment/Map format and SAMtools. Bioinformatics *25*, 2078–2079.

Liao, Y., Smyth, G.K., and Shi, W. (2014). featureCounts: an efficient general purpose program for assigning sequence reads to genomic features. Bioinformatics *30*, 923–930.

Libina, N., Berman, J.R., and Kenyon, C. (2003). Tissue-specific activities of *C. elegans* DAF-16 in the regulation of lifespan. Cell *115*, 489–502.

Lin, K., Hsin, H., Libina, N., and Kenyon, C. (2001). Regulation of the *Caenorhabditis elegans* longevity protein DAF-16 by insulin/IGF-1 and germline signaling. Nat. Genet. *28*, 139–145.

Love, M.I., Huber, W., and Anders, S. (2014). Moderated estimation of fold change and dispersion for RNA-seq data with DESeq2. Genome Biol. *15*, 550.

Machanick, P., and Bailey, T.L. (2011). MEME-ChIP: motif analysis of large DNA datasets. Bioinformatics *27*, 1696–1697.

Mann, R.S., and Chan, S.K. (1996). Extra specificity from extradenticle: the partnership between HOX and PBX/EXD homeodomain proteins. Trends Genet. *12*, 258–262.

Melo, J.A., and Ruvkun, G. (2012). Inactivation of conserved *C. elegans* genes engages pathogen- and xenobiotic-associated defenses. Cell *149*, 452–466.

Murphy, C.T., McCarroll, S.A., Bargmann, C.I., Fraser, A., Kamath, R.S., Ahringer, J., Li, H., and Kenyon, C. (2003). Genes that act downstream of DAF-16 to influence the lifespan of *Caenorhabditis elegans*. Nature *424*, 277–283.

O'Rourke, E.J., Soukas, A.A., Carr, C.E., and Ruvkun, G. (2009). *C. elegans* major fats are stored in vesicles distinct from lysosome-related organelles. Cell Metab. *10*, 430–435.

Ogg, S., Paradis, S., Gottlieb, S., Patterson, G.I., Lee, L., Tissenbaum, H.A., and Ruvkun, G. (1997). The Fork head transcription factor DAF-16 transduces insulin-like metabolic and longevity signals in *C. elegans*. Nature *389*, 994–999.

Pan, D., and Courey, A.J. (1992). The same dorsal binding site mediates both activation and repression in a context-dependent manner. EMBO J. 111837–111842.

Papp, D., Csermely, P., and Soti, C. (2012). A role for SKN-1/Nrf in pathogen resistance and immunosenescence in *Caenorhabditis elegans*. PLoS Pathog. *8*, e1002673.

Pauli, F., Liu, Y., Kim, Y.A., Chen, P.J., and Kim, S.K. (2006). Chromosomal clustering and GATA transcriptional regulation of intestine-expressed genes in *C. elegans*. Development *133*, 287–295.

Pukkila-Worley, R., Feinbaum, R., Kirienko, N.V., Larkins-Ford, J., Conery, A.L., and Ausubel, F.M. (2012). Stimulation of host immune defenses by a small molecule protects *C. elegans* from bacterial infection. PLoS Genet. *8*, e1002733.

Pukkila-Worley, R., Feinbaum, R.L., McEwan, D.L., Conery, A.L., and Ausubel, F.M. (2014). The evolutionarily conserved mediator subunit MDT-15/MED15 links protective innate immune responses and xenobiotic detoxification. PLoS Pathog. *10*, e1004143.

Quinlan, A.R., and Hall, I.M. (2010). BEDTools: a flexible suite of utilities for comparing genomic features. Bioinformatics *26*, 841–842.

Ramirez, F., Ryan, D.P., Gruning, B., Bhardwaj, V., Kilpert, F., Richter, A.S., Heyne, S., Dundar, F., and Manke, T. (2016). deepTools2: a next generation web server for deep-sequencing data analysis. Nucleic Acids Res. *44*, W160–W165.

Reece-Hoyes, J.S., Shingles, J., Dupuy, D., Grove, C.A., Walhout, A.J.M., Vidal, M., and Hope, I.A. (2007). Insight into transcription factor gene duplication from *Caenorhabditis elegans* promoterome-driven expression patterns. BMC Genomics *8*, 27.

Rieckhof, G.E., Casares, F., Ryoo, H.D., Abu-Shaar, M., and Mann, R.S. (1997). Nuclear translocation of extradenticle requires homothorax, which encodes an extradenticle-related homeodomain protein. Cell *91*, 171–183.

Robida-Stubbs, S., Glover-Cutter, K., Lamming, D.W., Mizunuma, M., Narasimhan, S.D., Neumann-Haefelin, E., Sabatini, D.M., and Blackwell, T.K. (2012). TOR signaling and rapamycin influence longevity by regulating SKN-1/Nrf and DAF-16/FoxO. Cell Metab. *15*, 713–724.

Saleh, M., Rambaldi, I., Yang, X.J., and Featherstone, M.S. (2000). Cell signaling switches HOX-PBX complexes from repressors to activators of transcription mediated by histone deacetylases and histone acetyltransferases. Mol. Cell. Biol. *20*, 8623–8633.

Schindelin, J., Arganda-Carreras, I., Frise, E., Kaynig, V., Longair, M., Pietzsch, T., Preibisch, S., Rueden, C., Saalfeld, S., Schmid, B., et al. (2012). Fiji: an open-source platform for biological-image analysis. Nat. Methods *9*, 676–682.

Schwartz, M.L., and Jorgensen, E.M. (2016). SapTrap, a Toolkit for High-Throughput CRISPR/Cas9 Gene Modification in *Caenorhabditis elegans*. Genetics *202*, 1277–1288.

Seah, N.E., de Magalhaes Filho, C.D., Petrashen, A.P., Henderson, H.R., Laguer, J., Gonzalez, J., Dillin, A., Hansen, M., and Lapierre, L.R. (2016). Autophagy-mediated longevity is modulated by lipoprotein biogenesis. Autophagy *12*, 261–272.

Shapira, M., Hamlin, B.J., Rong, J., Chen, K., Ronen, M., and Tan, M.W. (2006). A conserved role for a GATA transcription factor in regulating epithelial innate immune responses. Proc. Natl. Acad. Sci. USA *103*, 14086–14091.

Tan, M.W., Mahajan-Miklos, S., and Ausubel, F.M. (1999). Killing of *Caenorhabditis elegans* by *Pseudomonas aeruginosa* used to model mammalian bacterial pathogenesis. Proc. Natl. Acad. Sci. USA *96*, 715–720.

Tepper, R.G., Ashraf, J., Kaletsky, R., Kleemann, G., Murphy, C.T., and Bussemaker, H.J. (2013). PQM-1 complements DAF-16 as a key transcriptional regulator of DAF-2-mediated development and longevity. Cell *154*, 676–690.

Thyagarajan, B., Blaszczak, A.G., Chandler, K.J., Watts, J.L., Johnson, W.E., and Graves, B.J. (2010). ETS-4 is a transcriptional regulator of life span in *Caenorhabditis elegans*. PLoS Genet. *6*, e1001125.

Tullet, J.M., Hertweck, M., An, J.H., Baker, J., Hwang, J.Y., Liu, S., Oliveira, R.P., Baumeister, R., and Blackwell, T.K. (2008). Direct inhibition of the longevity-promoting factor SKN-1 by insulin-like signaling in *C. elegans*. Cell *132*, 1025–1038.

Van Auken, K., Weaver, D., Robertson, B., Sundaram, M., Saldi, T., Edgar, L., Elling, U., Lee, M., Boese, Q., and Wood, W.B. (2002). Roles of the Homothorax/Meis/Prep homolog UNC-62 and the Exd/Pbx homologs CEH-20 and CEH-40 in *C. elegans* embryogenesis. Development *129*, 5255–5268.

Van Nostrand, E.L., Sanchez-Blanco, A., Wu, B., Nguyen, A., and Kim, S.K. (2013). Roles of the developmental regulator *unc-62*/Homothorax in limiting longevity in *Caenorhabditis elegans*. PLoS Genet. *9*, e1003325.

Van Rompay, L., Borghgraef, C., Beets, I., Caers, J., and Temmerman, L. (2015). New genetic regulators question relevance of abundant yolk protein production in *C. elegans*. Sci. Rep. *5*, 16381.

Wahlby, C., Conery, A.L., Bray, M.A., Kamentsky, L., Larkins-Ford, J., Sokolnicki, K.L., Veneskey, M., Michaels, K., Carpenter, A.E., and O'Rourke, E.J. (2014). High- and low-throughput scoring of fat mass and body fat distribution in *C. elegans*. Methods *68*, 492–499.

Yang, L., Sym, M., and Kenyon, C. (2005). The roles of two *C. elegans* HOX cofactor orthologs in cell migration and vulva development. Development *132*, 1413–1428.

Zhang, J., Hashmi, S., Cheema, F., Al-Nasser, N., Bakheet, R., Parhar, R.S., Al-Mohanna, F., Gaugler, R., Hussain, M.M., and Hashmi, S. (2013). Regulation of lipoprotein assembly, secretion and fatty acid beta-oxidation by Kruppel-like transcription factor, *klf-3*. J. Mol. Biol. *425*, 2641–2655.

Zhang, Y., Liu, T., Meyer, C.A., Eeckhoute, J., Johnson, D.S., Bernstein, B.E., Nusbaum, C., Myers, R.M., Brown, M., Li, W., et al. (2008). Model-based analysis of ChIP-seq (MACS). Genome Biol. *9*, R137.

Zhou, K.I., Pincus, Z., and Slack, F.J. (2011). Longevity and stress in *Caenorhabditis elegans*. Aging (Albany, NY) *3*, 733–753.

STAR★METHODS

KEY RESOURCES TABLE

REAGENT or RESOURCE	SOURCE	IDENTIFIER
Antibodies		
Rat monoclonal anti-HA (clone 3F10)	Sigma-Aldrich	Cat# 11867423001; RRID:AB_390918
Mouse monoclonal anti-HA-Agarose (clone 2-2.2.14)	Thermo Fisher Scientific	Cat# 26181; RRID:AB_2537081
Mouse monoclonal anti-FLAG (clone M2)	Sigma-Aldrich	Cat# F1804; RRID:AB_262044
Mouse monoclonal anti-GFP (clone 3E6)	Thermo Fisher Scientific	Cat# A-11120; RRID:AB_221568
Mouse monoclonal anti-Actin (clone ACTN05)	Abcam	Cat# ab3280; RRID:AB_303668
Bacterial and Virus Strains		
E. coli: OP50	*Caenorhabditis* Genetics Center	RRID:WB-STRAIN:OP50
E. coli: HT115(DE3)	*Caenorhabditis* Genetics Center	RRID:WB-STRAIN:HT115(DE3)
Pseudomonas aeruginosa: PA14	Read Pukkila-Worley	RRID:WB-STRAIN:PA14
Chemicals, Peptides, and Recombinant Proteins		
2-Log DNA ladder	New England BioLabs	Cat# N3200S
Phusion	New England BioLabs	Cat# M0530S
Isopropyl-β-D-thiogalactoside	Gold Biotechnology	Cat# I2481C100
Oil Red O	Sigma-Aldrich	Cat# O9755
Trizol	Thermo Fisher Scientific	Cat# 15596018
Protein G Dynabeads	Thermo Fisher Scientific	Cat# 10003D
5-Fluoro-2'-deoxyuridine	Sigma-Aldrich	Cat# F0503
Formaldehyde (37%)	Sigma-Aldrich	Cat# F1635
Formaldehyde (16%)	Thermo Fisher Scientific	Cat# 28906
Proteinase K	New England BioLabs	Cat# P8107S
RNAseA	Sigma-Aldrich	Cat# R4642
Phenol:chloroform:isoamyl alcohol	Thermo Fisher	Cat# 15593031
Critical Commercial Assays		
Gibson Assembly Cloning Kit	New England BioLabs	Cat# E5510S
TURBO DNA-free kit	Thermo Fisher Scientific	Cat# AM1907
SuperScript III kit	Thermo Fisher Scientific	Cat# 18080051
PowerUp SYBR Green master mix	Thermo Fisher Scientific	Cat# A25742
TruSeq RNA Library Prep Kit v2	Illumina	Cat# RS-122-2001, RS-122-2002
KAPA Hyper Prep Kit	Kapa Biosystems	Cat# KR0961
ThruPLEX DNA-seq Kit	Rubicon Genomics	Cat# R400428
Deposited Data		
Raw and processed ChIP-Seq and mRNA-Seq data	This paper	GEO: GSE112981
Experimental Models: Organisms/Strains		
C. elegans: Strain N2 Bristol	*Caenorhabditis* Genetics Center	WB Strain: N2
C. elegans: Strain GR2122: *mgIs70[Pvit-3::GFP]*	Dowen et al., 2016	N/A
C. elegans: Strain DLS99: *ceh-60(ok1485) X; mgIs70[Pvit-3::GFP]*	This paper	N/A
C. elegans: Strain DLS357: *ceh-60(ok1485) X** *This strain is a 4x backcrossed version of VC988	This paper	N/A
C. elegans: Strain DH1390: *rme-2(b1008) IV*	*Caenorhabditis* Genetics Center	WB Strain: DH1390; WormBase: WBVar00000414

(*Continued on next page*)

Continued

REAGENT or RESOURCE	SOURCE	IDENTIFIER
C. elegans: Strain DLS400: *unc-119(ed3) III; rhdEx82[*Pceh-60::mCherry::unc-54 3'UTR + cb-unc-119(+)*]*	This paper	N/A
C. elegans: Strain DLS395: *ceh-60(rhd116 [3xHA-mCherry::ceh-60]) X*	This paper	N/A
C. elegans: Strain DLS406: *glo-4(ok623) V; ceh-60(rhd116[3xHA-mCherry::ceh-60]) X*	This paper	N/A
C. elegans: Strain DLS128: *ceh-60(ok1485) X; mgIs70*[Pvit-3::GFP]*; rhdEx24*[Pvha-6::mCherry:: SL2::ceh-60 + cb-unc-119(+)]	This paper	N/A
C. elegans: Strain DLS131: *ceh-60(ok1485) X; mgIs70*[Pvit-3::GFP]*; rhdEx27*[Psng-1::mCherry:: SL2::ceh-60 + cb-unc-119(+)]	This paper	N/A
C. elegans: Strain DLS387: *rhdSi31[*Pvha-6:: mCherry::SL2::ceh-60 + cb-unc-119(+)]/+ II; ceh-60(ok1485) X*	This paper	N/A
C. elegans: Strain DLS389: *rhdSi33[*Psng-1:: mCherry::SL2::ceh-60 + cb-unc-119(+)] II; ceh-60(ok1485) X*	This paper	N/A
C. elegans: Strain MGH171: *sid-1(qt9) V; alxIs7[*Pvha-6::sid-1::SL2::GFP*]*	Melo and Ruvkun, 2012	N/A
C. elegans: Strain DLS375: *sid-1(qt9) V; ceh-60(ok1485) X; alxIs7[*Pvha-6::sid-1:: SL2::GFP*]*	This paper	N/A
C. elegans: Strain DLS404: *rme-2(b1008) IV; ceh-60(ok1485) X*	This paper	N/A
C. elegans: Strain GR1329: *daf-16(mgDf47) I*	Ogg et al., 1997	N/A
C. elegans: Strain DLS405: *daf-16(mgDf47) I; ceh-60(ok1485) X*	This paper	N/A
C. elegans: Strain EU31: *skn-1(zu135) IV/nT1 [unc-?(n754) let-?] (IV;V)*	*Caenorhabditis* Genetics Center	WB Strain: EU31; WormBase: WBVar00275492
C. elegans: Strain DLS403: *skn-1(zu135) IV/nT1 [unc-?(n754) let-?] (IV;V); ceh-60(ok1485) X*	This paper	N/A
C. elegans: Strain DLS359: *pqm-1(ok485) II; ceh-60(ok1485) X; mgIs70*[Pvit-3::GFP]	This paper	N/A
C. elegans: Strain DLS360: *daf-16(mgDf47) I; ceh-60(ok1485) X; mgIs70*[Pvit-3::GFP]	This paper	N/A
C. elegans: Strain DLS361: *daf-16(mgDf47) I; pqm-1(ok485) II; ceh-60(ok1485) X; mgIs70 [*Pvit-3::GFP*]*	This paper	N/A
C. elegans: Strain DLS396: *ceh-60(rhd116 [3xHA-mCherry::ceh-60]) X; gaIs285[*Punc-62:: unc-62(7a)::TY1-eGFP-3xFLAG + unc-119(+)*]*	This paper	N/A
C. elegans: Strain DLS397: *glo-4(ok623) V; ceh-60(rhd116[3xHA-mCherry::ceh-60]) X; gaIs285[*Punc-62::unc-62(7a)::TY1-eGFP-3xFLAG + unc-119(+)*]*	This paper	N/A
C. elegans: Strain SD1890: *glo-4(ok623) V; gaIs285[*Punc-62::unc-62(7a)::TY1-eGFP-3xFLAG + unc-119(+)*]*	*Caenorhabditis* Genetics Center	WB Strain: SD1890; WormBase: WBVar00091907
C. elegans: Strain KU25: *pmk-1(km25) IV*	*Caenorhabditis* Genetics Center	WB Strain: KU25; WormBase: WBVar00088252
C. elegans: Strain AU307: *agIs44[*Pirg-4:: GFP::unc-54 3'UTR + Pmyo-2::mCherry*]*	Pukkila-Worley et al., 2014	N/A

(*Continued on next page*)

Continued

REAGENT or RESOURCE	SOURCE	IDENTIFIER
C. elegans: Strain DLS410: *ceh-60(ok1485) X; agIs44 [Pirg-4::GFP::unc-54 3'UTR + Pmyo-2::mCherry]*	This paper	N/A
C. elegans: Strain DLS420: *pqm-1(ok485) II; ceh-60(ok1485) X*	This paper	N/A
C. elegans: Strain DLS421: *pqm-1(ok485) II*	This paper	N/A
C. elegans: Strain DLS423: *pqm-1(rhd90[T266A, S267A, T268A]) II; ceh-60(ok1485) X*	This paper	N/A
C. elegans: Strain DLS424: *pqm-1(rhd90[T266A, S267A, T268A]) II*	This paper	N/A
C. elegans: Strain DLS435: *pqm-1(ok485) II; ceh-60(rhd116[3xHA::mCherry::ceh-60]) X*	This paper	N/A
C. elegans: Strain OP201: *unc-119(tm4063) III; wgIs201[PQM-1::TY1::EGFP::3xFLAG(92C12) + unc-119(+)]*	*Caenorhabditis* Genetics Center	WB Strain: OP201; WormBase: WBVar00252617
C. elegans: Strain DLS422: *ceh-60(ok1485) X; wgIs201[PQM-1::TY1::EGFP::3xFLAG(92C12) + unc-119(+)]*	This paper	N/A
C. elegans: Strain DLS448: *ceh-60(rhd116[3xHA-mCherry::ceh-60]) X; wgIs201[PQM-1::TY1::EGFP::3xFLAG(92C12) + unc-119(+)]*	This paper	N/A
C. elegans: Strain HT1593: *unc-119(ed3)* III	*Caenorhabditis* Genetics Center	WB Strain: HT1593; WormBase: WBVar00145093
C. elegans: Strain EG6699: *ttTi5605* II; *unc-119(ed3)* III	*Caenorhabditis* Genetics Center	WB Strain: EG6699; WormBase: WBVar00145093
Oligonucleotides		
Primers used in this study are listed in Table S1	This paper	N/A
Recombinant DNA		
Ahringer *C. elegans* RNAi plasmid: control RNAi: pL4440	Addgene	Cat# 1654
Ahringer *C. elegans* RNAi plasmid: *vit-1/2* RNAi: pL4440(*vit-1/2*)	This paper	N/A
Ahringer *C. elegans* RNAi plasmid: *vit-3/4/5* RNAi: pL4440(*vit-3/4/5*)	Source BioScience	https://www.sourcebioscience.com/products/life-sciences-research/clones/rnai-resources/c-elegans-rnai-collection-ahringer/
Ahringer *C. elegans* RNAi plasmid: *vit-6* RNAi: pL4440(*vit-6*)	Source BioScience	https://www.sourcebioscience.com/products/life-sciences-research/clones/rnai-resources/c-elegans-rnai-collection-ahringer/
Ahringer *C. elegans* RNAi plasmid: *ceh-60* RNAi: pL4440(*ceh-60*)	Source BioScience	https://www.sourcebioscience.com/products/life-sciences-research/clones/rnai-resources/c-elegans-rnai-collection-ahringer/
Ahringer *C. elegans* RNAi plasmid: *unc-62* RNAi: pL4440(*unc-62*)	Source BioScience	https://www.sourcebioscience.com/products/life-sciences-research/clones/rnai-resources/c-elegans-rnai-collection-ahringer/
Plasmid: pCFJ151	Addgene	Cat# 19330
Plasmid: pMLS256	Addgene	Cat# 73715
Plasmid: pMLS328	Addgene	Cat# 73717
Plasmid: pDD162	Dickinson et al., 2013	N/A
Software and Algorithms		
STAR	Dobin et al., 2013	https://github.com/alexdobin/STAR
Subread, featureCounts	Liao et al., 2014	http://bioinf.wehi.edu.au/featureCounts/
DESeq2	Love et al., 2014	http://bioconductor.org/packages/DESeq2/

(*Continued on next page*)

Continued

REAGENT or RESOURCE	SOURCE	IDENTIFIER
bowtie2	Langmead and Salzberg, 2012	http://bowtie-bio.sourceforge.net/bowtie2/index.shtml
SAMtools	Li et al., 2009	http://samtools.sourceforge.net/
deepTools	Ramirez et al., 2016	https://github.com/deeptools/deepTools
MACS2	Zhang et al., 2008	https://github.com/taoliu/MACS/wiki/Install-macs2
bedtools	Quinlan and Hall, 2010	https://github.com/arq5x/bedtools2
DAVID	Huang da et al., 2009	https://david.ncifcrf.gov/
MEME-ChIP	Machanick and Bailey, 2011	http://meme-suite.org/tools/meme-chip
CentriMo	Bailey and Machanick, 2012	http://meme-suite.org/tools/centrimo

CONTACT FOR REAGENT AND RESOURCE SHARING

Further information and requests for resources and reagents should be directed to and will be fulfilled by the Lead Contact, Robert Dowen (dowen@email.unc.edu).

EXPERIMENTAL MODEL AND SUBJECT DETAILS

All *C. elegans* strains were maintained on NGM media seeded with *E. coli* OP50 (Brenner, 1974). The mutant and transgenic strains used in this study are described in the Key Resources Table. For RNAi experiments, animals were fed *E. coli* HT115(DE3) carrying the L4440 RNAi plasmid (See RNAi experiments). Unless noted otherwise, animals were grown at 20°C for experimentation and only hermaphrodite animals were analyzed.

METHOD DETAILS

Generation of Transgenic Strains

The *ceh-60* transcriptional reporter was assembled in the pCFJ151 plasmid (Frokjaer-Jensen et al., 2008) by fusing 3,513 bp of sequence upstream of the *ceh-60* transcriptional start site to *mCherry::unc-54 3′UTR* by Gibson assembly (Gibson et al., 2009). The plasmid was microinjected into the HT1593 strain at 20 ng/μl with 80 ng/μl of 2-Log DNA ladder (New England BioLabs) to generate the DLS400 strain. Multiple independent transgenic lines displayed a similar mCherry expression pattern.

N-terminal epitope tagging of the endogenous *ceh-60* gene was performed by genome editing using CRISPR/Cas9 technology (Dickinson et al., 2013). Homology arms (HA, 57 bp long) were fused to the 3xHA epitope tag and the mCherry gene using SapTrap to generate *5'HA::3xHA::mCherry-unc-119::N-tag-CNCTR::3'HA* in the pMLS256 2-site destination plasmid (Schwartz and Jorgensen, 2016). A sgRNA sequence targeting the 5' end of the *ceh-60* gene (5'-TCACACCGATCTTTGAGAGATGG-3') was simultaneously introduced into pMLS256 during the SapTrap reaction. The resulting plasmid was microinjected into HT1593 along with the P*eft-3::Cas9* plasmid pDD162 (Dickinson et al., 2013). Non-Unc integrants were microinjected with pMLS328 (P*eft-3::Cre*) to remove the *LoxP::unc-119::LoxP* selectable marker, and proper genome editing was confirmed by Sanger sequencing of a PCR product amplified from the edited region. The resulting strain was backcrossed 3x to N2 to remove the *unc-119(ed3)* mutation.

The *ceh-60* tissue-specific rescue constructs were generated by fusing the intestinal-specific *vha-6* promoter (934 bp) or the pan-neuronal *sng-1* promoter (1,967 bp) to a *mCherry::his-58::SL2* cassette fused to the *ceh-60* genomic locus (9,070 bp downstream of the transcriptional start site). The SL2-specific trans-splice site was used to infer the tissue-specificity of *ceh-60* expression, as previously described (Dowen et al., 2016). The DNA fragments (promoters, *mCherry::his-58::SL2* cassette, and *ceh-60*) were individually amplified by PCR (Phusion, New England BioLabs), and assembled into the MosSCI-compatible pCFJ151 plasmid (Frokjaer-Jensen et al., 2008) by Gibson assembly (Gibson et al., 2009). The resulting constructs were verified by Sanger sequencing and microinjected into DLS99 (20 ng/μl plasmid, 80 ng/μl of DNA ladder) to generate DLS128 and DLS131. Similar results were observed using multiple independent transgenic lines. To generate single-copy rescue strains using MosSCI, the P*vha-6::mCherry::his-58::SL2*::*ceh-60* and P*sng-1::mCherry::his-58::SL2::ceh-60* plasmids were individually microinjected into EG6699 as previously described (Frokjaer-Jensen et al., 2008). Single-copy integrants were crossed to DLS357 to generate DLS387 and DLS389. Strains carrying the *rhdSi31* [P*vha-6::mCherry::SL2::ceh-60* + *cb-unc-119(+)*] allele were maintained as a heterozygote because homozygous animals are sterile.

Imaging of Transgenic Animals

Transgenic worms carrying the P*vit-3*::*GFP* the reporter were imaged with a 10x objective on a Zeiss Axio Imager Z1 microscope running the AxioVision 4.6 software (Figures 1A and 2C) or a Nikon Eclipse E800 microscope running the NIS Elements 4.51 software (Figure S1A). Images of all additional transgenic animals, as well as all brightfield images, were generated with the Nikon Eclipse E800 microscope.

RNAi Experiments

Individual RNAi clones for gene knockdown experiments were obtained from the Ahringer RNAi library and were confirmed by Sanger sequencing. A homemade RNAi clone targeting a coding sequence shared by the *vit-1* and *vit-2* genes was constructed by amplifying the region from N2 worm genomic DNA prior to cloning the fragment into the empty L4440 vector (Addgene) using standard cloning techniques. Knockdown of all six *vit* genes was achieved by pooling the *vit-1/2*, *vit-3/4/5* (Ahringer), and *vit-6* (Ahringer) clones in equal parts prior to seeding the RNAi plates. The L4440 empty vector was included in all experiments as the RNAi negative control. The RNAi strains were grown overnight in Luria–Bertani medium containing ampicillin (50 μg/ml), concentrated 20-25x by centrifugation, and seeded on NGM plates containing 5 mM isopropyl-β-D-thiogalactoside (IPTG) and ampicillin (50 μg/ml). The plates were incubated at room temperature overnight to induce expression of the dsRNAs. After bleaching adult animals, L1 larvae were synchronized overnight in M9 buffer prior to dropping them on RNAi plates. The animals were incubated at 20°C for ~72 hr prior to processing. For longevity assays, well-fed animals grown on OP50 until adulthood were transferred to the RNAi plates and allowed eggs for ~8 hr, and the animals from the following generation were used for the longevity experiments.

Oil Red O Staining

Adult animals were harvested in S buffer, fixed with 60% isopropanol, stained with 0.3% Oil Red O in 60% isopropanol for 6 hr (intestinal imaging) or 16 hr (embryo imaging), washed with S buffer containing 0.01% Triton X-100, and mounted on 2% agarose pads for imaging exactly as previously described (Wahlby et al., 2014). Stained animals were imaged with a 10x objective on a Nikon Eclipse E800 microscope using a monochrome digital camera.

Image Analysis

Quantification of Oil Red O and brightfield images was performed with ImageJ (Schindelin et al., 2012). For analysis of embryos, all visible eggs in the uterus of each animal were outlined using the freehand selection tool prior to measuring the mean pixel intensity for the selected area. For intestinal measurements, the head of each animal was cropped from the image (1000 x 250 pixels, see Figure S1B), the intestine was outlined using the wand tool, and mean pixel intensity was measured. Background measurements were performed for each image. The mean background-subtracted pixel intensity and standard deviation for each population was calculated.

Quantitative PCR

L1 animals were synchronized by egg prep and grown on OP50 for ~72 hr at 20°C until they reached the first day of adulthood. Animals were harvested in M9 buffer, washed, and flash frozen. When dealing with a segregating population (Figures 2D and S4E), animals (100-200 per genotype) were directly picked to M9 buffer. Total RNA was isolated using Trizol and the residual gDNA was removed using the TURBO DNA-free kit per the manufacturer's instructions (Thermo Fisher). The cDNA was synthesized by oligo(dT) priming using the SuperScript III kit according to the manufacturer's instructions (Thermo Fisher). Quantitative PCR was performed on a QuantStudio 6 Flex Real-Time PCR System using the PowerUp SYBR Green master mix according to the manufacturer's recommendations (Thermo Fisher). For any given experimental sample, the C_T values for each target gene were first normalized to *act-1*. The resulting ΔC_T value was averaged across three independently performed experiments and the standard error of the mean (ΔC_T SEM) was calculated. The $\Delta\Delta C_T$ values were calculated by normalization to a wild-type control sample and the error was propagated using the formula $[(\Delta C_T\ SEM_{control})^2 + (\Delta C_T\ SEM_{test})^2]^{1/2}$. The mean and SEM values were then transformed using $2^{-\Delta\Delta CT}$.

Western Blot Analyses

Animals were harvested in M9 buffer, washed, and resuspended in Laemmli buffer. The samples were boiled, resolved by SDS-PAGE, and transferred to a nitrocellulose or PVDF membrane. Blots were probed with either anti-FLAG (M2, Sigma), anti-HA (3F10, Sigma), or anti-Actin antibodies (Abcam).

For co-immunoprecipitation assays (Figures 5H, 7D, and S7B), ~50,000 animals were harvested in water, washed, and ground to a fine power in liquid nitrogen. The ground worms were resuspended in cell lysis buffer (50 mM Tris-HCl pH 7.5, 100 mM KCl, 2.5 mM $MgCl_2$, 0.1% NP-40, protease inhibitors), homogenized by sonication using a Bioruptor Plus (Diagenode, 30 sec on/off cycles, 10 cycles; Figure 5H) or a Covaris E220 (4 min; Figures 7D and S7B), and the lysate was cleared by centrifugation. Proteins were immunoprecipitated overnight at 4°C from the lysates using anti-HA-Agarose beads (Pierce) or anti-FLAG (Sigma) bound to Protein G Dynabeads (Thermo Fisher). The beads were washed with lysis buffer, resuspended in Laemmli buffer, and Western blotting was performed as described above.

Lifespan and Brood Size Assays

To avoid any transgenerational starvation effects, animals were reared on an abundance of food for at least two generations prior to being assayed. Adults were transferred to new plates daily during the reproductive period to avoid overpopulation and starvation. Following reproduction, animals were maintained on uncontaminated plates (25 animals/plate, 100-125 total animals) and were scored daily for movement during the length of the assay. Animals that burst, bagged, or crawled off the plate were censored. To determine whether motionless animals were indeed alive, animals were gently touched on the head with a pick to induce movement.

For brood size assays, animals were grown identically to those animals in the lifespan assays. At least ten L4 animals were picked to individual plates and transferred daily throughout the reproductive period. Laid embryos were allowed to develop into L3/L4s before they were counted. Data are reported as the mean +/- the standard deviation.

Pseudomonas aeruginosa Assays

Well-fed adult animals were allowed to lay embryos on NGM plates seeded with OP50. The resulting animals were allowed to develop to the L4 stage at 20°C before they moved to NGM-OP50 plates containing 1 mg/ml 5-Fluoro-2'-deoxyuridine (Sigma). ''Slow killing'' *Pseudomonas aeruginosa* PA14 infection assays were performed at 25°C using day 1 adult animals as previously described (Pukkila-Worley et al., 2012). Animals (~50 animals/plate, 5 replicate plates/genotype) were scored for viability by gentle touch at least once per day. For the survival plots, individual data points are reported as the mean +/- the standard deviation.

For RT-qPCR assays, day 1 adult animals were picked to slow killing plates containing *Pseudomonas*. Animals were exposed to pathogen for 8 hr at 25°C before they were harvested in M9 buffer, washed, and flash frozen in Trizol.

Chromatin Immunoprecipitation

ChIP experiments were performed on strains DLS395 (Figures 4A, 4C, 7A–7C, 7E, S7A, and S7C), DLS396 (Figures 5A, 5C, 5D, 6C, and 6D), DLS435 (Figure S7C), OP201 (Figures 7E, S7D, and S7G), and DLS422 (Figure S7D). Synchronized animals were grown to day 1 adults (see Quantitative PCR) before they were harvested in M9 buffer, washed, flash frozen in PBS as small droplets in liquid nitrogen, and ground to a fine powder using a mortar and pestle. Samples (~20,000 worms/ml) were crosslinked in 2% formaldehyde (F1635, Sigma) for 30 minutes (Figures 4, 5, 6, 7A–7C, and S7G) or 1% formaldehyde (28906, Thermo Fisher) for 5 minutes (Figures 7E, S7C, S7D, and S7G) at room temperature before quenching with 125 mM glycine. The chromatin was washed with PBS, resuspended in ChIP lysis buffer (50 mM Hepes pH 7.5, 300 mM NaCl, 1 mM EDTA, 1% Triton X-100, 0.1% sodium deoxycholate, 0.5% N-lauroylsarcosine, protease inhibitors), and sheared using a Bioruptor Plus (Diagenode, 30 sec on/off cycles, 20 cycles; Figures 4, 5, 6, 7A–7C, and S7G) or a Covaris E220 (4 min; Figures 7E, S7C, S7D, and S7G). Cleared lysates were immunoprecipitated with either anti-HA (3F10, Sigma; Figures 4A, 4C, 5A, 5C, 5D, 6C, 7A–7F, S7A, S7C, and S7G), anti-GFP (3E6, Thermo Fisher), or anti-FLAG (M2, Sigma) antibodies bound to Protein G Dynabeads (Thermo Fisher), or alternatively, with anti-HA-Agarose beads (mIgG1, Pierce; Figures 4A, 4C, and 7C only). The beads were washed (5 min at 4°C) twice with ChIP lysis buffer, once with high salt ChIP lysis buffer (ChIP lysis buffer containing 800 mM NaCl), twice with LiCl ChIP buffer (10 mM Tris-HCl pH 8.0, 250 mM LiCl, 0.5 % NP-40, 0.5 % sodium deoxycholate, 1 mM EDTA), and once with low salt TE (10 mM Tris-HCl pH 8.0, 1 mM EDTA, 50 mM NaCl). The chromatin was eluted (50 mM Tris–HCl pH 8.0, 10mM EDTA, 1% SDS) and the crosslinks were reversed by incubation at 65°C overnight. The DNA samples were treated with RNAseA (Sigma) and Proteinase K (New England BioLabs), extracted with phenol:chloroform:isoamyl alcohol (Thermo Fisher), ethanol precipitated, and resuspended in buffer EB (Qiagen).

Library Preparation

mRNA-Seq libraries were prepared from 1 μg of total RNA (see Quantitative PCR) using the TruSeq RNA Library Prep Kit v2 according to the manufacturer's instructions (Illumina). Three independent biological replicates were prepared for each condition. The ChIP-Seq libraries were prepared using the ThruPLEX DNA-Seq Kit per the manufacturer's instructions (Rubicon Genomics; Figures 7E, S7C, S7D, and S7G) or by the High Throughput Genomic Sequencing Facility at the University of North Carolina at Chapel Hill using the KAPA Hyper Prep Kit (Kapa Biosystems; Figures 4, 5, 6, 7A–7C, and S7G).

Sequencing Read Mapping and Downstream Processing

mRNA-Seq reads were aligned to the *C. elegans* genome (WS260) using the STAR aligner (Dobin et al., 2013) and gene-level read counts were calculated using the featureCounts algorithm of the subread package (Liao et al., 2014). Differential expression analyses were performed with the DESeq2 package using a 1% FDR cutoff (Love et al., 2014). Normalized and transformed gene-level counts, which were used to calculate transcriptome-wide differential expression, were calculated with the rlog algorithm of DESeq2.

The ChIP-Seq reads were mapped to the *C. elegans* genome (WS260) with bowtie2 (Langmead and Salzberg, 2012) using the default parameters. The SAMtools package (Li et al., 2009) was used to filter low quality reads (view -bS -q 10) and to remove duplicate reads (rmdup -s). Genome-wide ChIP enrichment was calculated relative to input (log_2 ratio) in 10 bp bins using the bamCompare module within the deepTools suite (Ramirez et al., 2016). ChIP-Seq peaks were called using processed reads from ChIP (''treatment'') and input (''control'') samples using MACS2 (Zhang et al., 2008) with the following parameters: -g ce –nomodel –extsize 175 –SPMR –keep-dup all -q 0.01.

To generate the UCSC genome browser tracks (https://genome.ucsc.edu), mRNA-Seq and ChIP-Seq reads were mapped to the WS235 genome build. mRNA-Seq reads from replicate samples were pooled, processed as described above, and BedGraph files were generated using the bedtools genomecov algorithm (Quinlan and Hall, 2010) with scaling to normalize for read count. BedGraph files for ChIP enrichment were generated with MACS2.

Genomic Data Correlations and Analyses

ChIP-Seq enrichment heatmaps or metagene plots were generated using the deepTools suite (computeMatrix, plotHeatmap, plotProfile) from the genome-wide ChIP enrichment files described above (bamCompare). The data were plotted relative to the transcriptional start sites of differentially expressed genes or ChIP-Seq peak summits (MACS2). For analyses utilizing the ChIP-Seq

peaks output by MACS2 (Figures 5D, 7E, 7F, S7C, and S7D), highly occupied target (HOT) regions, which are bound by a majority of transcription factors, as well as blacklisted regions were removed prior to analysis (Boyle et al., 2014; Encode Project Consortium, 2012). Lists of genes with expression enriched in the neurons (Kaletsky et al., 2016) or in the intestine, germline, and muscle (Pauli et al., 2006) have been described previously, and were used for analysis of specific subsets of genes. Differential expression at high confidence CEH-60/PQM-1 target genes (Figures 7F and S7H) was performed by selecting genes were that had a CEH-60/PQM-1 peak summit upstream of the transcriptional start site (<1000 bp) and that were differentially expressed in the *ceh-60(ok1485)/pqm-1(ok485)* mutant. The data were plotted using the R boxplot package using the default parameters (notch=T, outline=F).

For correlation of all modENCODE ChIP-Seq datasets (Figure 7B), reads from CEH-60 ChIP-Seq samples were mapped to the WS220 genome build before building genome-wide enrichment files with deepTools (100 bp bin size). Signal files for input and ChIP samples generated by the modENCODE project were downloaded and converted to bigWig files before calculating the genome-wide ChIP enrichment for each sample using deepTools (bigwigCompare, 100 bp bin size). After removal of HOT and blacklisted regions, ChIP enrichment surrounding the transcriptional start sites (+/- 2,500 bp) of genes differentially expressed in the *ceh-60(ok1485)* mutant was calculated for each sample using the multiBigwigSummary tool and the Pearson correlation for each pairwise comparison was calculated using the plotCorrelation tool (deepTools). Clustering and plotting of the Pearson correlation values was performed using the heatmap.2 function from the gplots R package.

Gene Ontology Enrichment

The gene ontology enrichment analyses (Biological Process, BP Direct) were performed on differentially expressed genes (1%FDR) using DAVID (Huang da et al., 2009).

Enriched Motif Analysis

To identify motifs enriched at CEH-60 peaks (DLS395 strain, anti-HA 3F10), ChIP-Seq peaks (MACS2) within the promoters (+/- 2,500 bp from TSS) of genes up- and/or down-regulated in the *ceh-60(ok1485)* mutant (day 1 adults) were selected as CEH-60 target genes. If multiple peaks were present within these regions, the peak with the strongest ChIP enrichment was selected for downstream analysis. Sequences surrounding the summits of these peaks (+/- 100 bp) were used for motif discovery using the MEME-ChIP software (Machanick and Bailey, 2011). The motif positional probabilities were calculated using CentriMo (Bailey and Machanick, 2012).

QUANTIFICATION AND STATISTICAL ANALYSIS

Statistical analyses of brightfield or Oil Red O images were performed using a Student's t-test (two sample comparison) or a one-way ANOVA with Bonferroni's multiple comparisons correction (more than two sample comparison). For RT-qPCR experiments, at least three independent biological replicates were generated for each experiment. Lifespan curves were compared using a Log-rank test. For determination of differential expression (RNA-Seq, DESeq2) or for identification of transcription factor binding sites (ChIP-Seq, MACS2), a 1% False Discovery Rate cutoff was applied. For enrichment calculations using gene lists (observed/expected, see Figure 4B), a hypergeometric test was performed to determine whether the enrichment/depletion was significant.

DATA AND SOFTWARE AVAILABILITY

Raw and processed data for all ChIP-Seq and mRNA-Seq datasets have been deposited. The accession number for the data reported in this paper is GEO: GSE112981.